https://doi.org/10.5194/egusphere-2026-2723
Preprint. Discussion started: 13 July 2026

Method-Dependent Variability in Hygroscopicity Parameter (κ) of Particles from Biomass-Burning Across Fuel Types and Burn Phases

Sara Aisyah Syafira[1,a], Dawei Hu[1], Aristeidis Voliotis[1,2], Huihui Wu[1,b], Osayomwanbor Ebenezer Oghama[1], Yunqi Shao[1], Sri Hapsari Budisulistiorini[3], Yu Wang[4], Michael Flynn[1], Peter James Gallimore[1], Hugh Coe[1,2], James Allan[1,2], and Gordon McFiggans[1]

[1]Centre for Atmospheric Science, Department of Earth and Environmental Sciences, School of Natural Sciences, University of Manchester, Manchester, M13 9PL, UK
[2]National Centre for Atmospheric Science (NCAS), University of Manchester, Manchester, M13 9PL, UK
[3]Wolfson Atmospheric Chemistry Laboratories, Department of Chemistry, University of York, UK
[4]School of Geosciences, University of Edinburgh, College of Science and Engineering, EH9 3JW, United Kingdom
[a]Now at: Research Centre for Climate and Atmosphere (PRIMA), National Research and Innovation Agency (BRIN), Indonesia
[b]Now at: Université Paris Cité and Univ Paris Est Créteil, CNRS, LISA, F-75013 Paris, France

Correspondence to: Sara Aisyah Syafira (sara005@brin.go.id) and Gordon McFiggans (g.mcfiggans@manchester.ac.uk)

Abstract. The hygroscopicity parameter κ is important for assessing biomass-burning aerosol impacts on visibility, direct radiative forcing, and cloud-related indirect effects. Discrepancies among κ values derived from different methods have been reported, but often separately across fuel types, burn phases, and experimental systems, limiting assessment of their consistency and controlling factors. Here, we compare κ derived from a cloud condensation nuclei counter (CCNC), a hygroscopicity tandem differential mobility analyzer (HTDMA), and AMS–SP2 composition-based predictions within a single laboratory framework. Fresh and aged biomass-burning particles were produced from four representative fuels: hardwood, softwood, peat, and leaves, burned under smouldering or flaming conditions. CCNC-derived κ systematically exceeded HTDMA-derived κ, with discrepancy magnitudes strongly dependent on fuel type and burn phase. Composition-based κ generally fell between CCNC and HTDMA values. Coupled effects of κ size dependence and size representation, together with externally mixed non-hygroscopic black carbon, affected discrepancies among the three approaches but only partly explained them. Using O:C-informed κ_{org} values instead of a constant $\kappa_{org} = 0.1$ consistently improved AMS–SP2 prediction accuracy relative to HTDMA values in peat experiments only, by 16–59%, while substantial residual discrepancies remained. These results suggest the presence of additional controlling factors not tested here, motivating measurements of surface-active species, particle phase state, and co-condensation of soluble gases to potentially explain the remaining discrepancies in future work. They further highlight the need for regime-aware κ parameterizations in atmospheric and climate models, alongside careful treatment of size representation, black-carbon inclusion, and κ_{org} assumptions in composition-based hygroscopicity predictions.

https://doi.org/10.5194/egusphere-2026-2723
Preprint. Discussion started: 13 July 2026

1. Introduction

Biomass-burning (BB) aerosol particles originate from both natural and anthropogenic combustion sources, including agricultural burning, biofuel use, and wildfires, and have well-established impacts on human health, air quality, and climate (Andrea, 2019; Noyes et al., 2022). One key property governing these impacts is hygroscopicity, which describes the ability of particles to absorb and retain water from the surrounding atmosphere (Tang et al., 2019). Hygroscopicity is controlled primarily by chemical composition and, to a lesser extent, by particle size, with subsequent feedback on particle properties during atmospheric processing (Wang et al., 2020; Wu et al., 2020). Through its influence on particle water-uptake behavior, hygroscopicity affects aerosol optical properties, aqueous-phase chemistry, and cloud–aerosol interactions under both subsaturated and supersaturated conditions (Petters and Kreidenweis, 2007; Zardini et al., 2008; Cai et al., 2018).

Under subsaturated conditions, hygroscopicity is commonly quantified via the hygroscopic growth factor (HGF), whereas under supersaturated conditions, it is inferred from the ability of particles to activate as cloud condensation nuclei (CCN), typically described by parameters such as critical supersaturation or activation diameter. These two regimes are associated with different atmospheric roles: subsaturated growth is closely linked to visibility degradation and near-surface radiative effects, while CCN activity governs cloud droplet formation and cloud radiative properties (Gysel et al., 2002; Wang et al., 2023). Correspondingly, HGF is usually measured using a hygroscopicity tandem differential mobility analyzer (HTDMA) (Swietlicki et al., 2008; Good et al., 2010), whereas CCN activity is measured using a differential mobility analyzer coupled with a cloud condensation nuclei counter (DMA–CCNC) (Tao et al., 2020). Both approaches enable direct, real-time measurements of submicron aerosol hygroscopic behavior, but they probe fundamentally different humidity regimes.

To bridge hygroscopicity characterization across subsaturated and supersaturated conditions, the single-parameter hygroscopicity framework, κ, was introduced (Petters and Kreidenweis, 2007). The κ parameter provides a unified description of particle water uptake and CCN activation behavior and has been widely adopted in aerosol–cloud interaction studies and climate modelling (Markelj et al., 2017). By design, κ simplifies the representation of hygroscopicity without requiring detailed molecular-level composition information, which is often difficult to obtain for complex atmospheric aerosols. For multicomponent particles, κ can be estimated using the Zdanovskii–Stokes–Robinson (ZSR) mixing rule as a volume-weighted sum of the hygroscopicity parameters of individual components (Petters and Kreidenweis, 2007).

When chemical composition data are available, κ can therefore be predicted using assumed fractional hygroscopicity values for organic and inorganic components, often derived from aerosol mass spectrometry (AMS) measurements. This composition-based approach has practical advantages, including high time resolution and operational simplicity relative to HTDMA and CCNC measurements, and allows simultaneous access to chemically resolved aerosol properties (Wang et al., 2020). Although

https://doi.org/10.5194/egusphere-2026-2723
Preprint. Discussion started: 13 July 2026

biomass-burning aerosols exhibit a wide range of reported κ values, spanning from near-hydrophobic to highly hygroscopic regimes (Alonso-Blanco et al., 2014), large compositional variability does not necessarily translate into large κ variability. For example, in organic-dominated aerosol regimes, κ is relatively insensitive to detailed molecular composition and depends primarily on the fraction of water-soluble, polar material (Petters and Kreidenweis, 2007; Mei et al., 2013; Haslett et al., 2019). As a result, AMS-based κ prediction is increasingly used in laboratory and field studies.

Despite the conceptual appeal of κ as a unifying parameter, the wide range of κ values reported for biomass-burning aerosols often shows limited comparability across studies, even when similar determination approaches are employed. Meanwhile, variability in combustion conditions, fuel types, and experimental protocols—particularly those related to sampling, dilution, and aging treatments—can strongly influence both initial and aged particle-phase and gas-phase compositions (Reid et al., 2005; Hennigan et al., 2011; Laskin et al., 2015; Li et al., 2019; Syafira et al., 2026), likely further affecting the resulting hygroscopicity. Across different κ determination methods (HTDMA, CCNC, and chemical-composition-based prediction) within the same or single experimental framework, discrepancies have been widely reported for various aerosol types (Gunthe et al., 2009; Jurányi et al., 2010; Mei et al., 2013). However, for biomass-burning aerosols, such discrepancies are typically discussed qualitatively and in isolation, often based on limited fuel sets, single burning conditions, or incomplete treatment of aging and BC effects (Levin et al., 2010; Engelhart et al., 2012).

A recent study (Bai et al., 2026) tested and found agreement between subsaturated κ and supersaturated κ obtained from density informed-QCM measurement and CCNC, respectively. However, it should not be interpreted as direct evidence that HTDMA-derived κ and CCNC-derived κ would also agree, because QCM and HTDMA rely on different subsaturated water-uptake measurements and retrieval assumptions. Additionally, though the fuel beds tested in their experiments were constructed to mimic or replicate the real fuel conditions, there were no important isolated tests on different fuel types, like wood versus peat, and different burn phases like flaming versus smouldering, to represent biomass burning under contrasting real-world burning conditions, such as Indonesian smouldering peat fires (Chen et al., 2017) and the more varied non peat wildland fires in California (Ward-Baranyay, et. al. 2025). All the tested smoke particles by (Bai et al., 2026) were composed predominantly of organics at 97–98% - the typical compositions for dominantly smouldering particles.

The present study, therefore, aims to provide a structured inter-method evaluation of κ values derived from HTDMA, CCNC, and AMS–SP2-based chemical-composition prediction within a single controlled experimental framework, allowing for separation from inter-study variability caused by different fuel and burn types, facilities, dilution histories, and ageing protocols. By comparing multiple fuel types (leaves, peat, softwood, and hardwood) and combustion phases (smouldering versus flaming), under uniformly applied fresh-to-aged conditions of up to 6 h, this work focuses on diagnosing the magnitude, direction, and consistency of κ discrepancies across methods. Systematic evaluation was conducted on the extent to which commonly invoked factors—including size representativeness, assumed component κ values, and black carbon treatment—

https://doi.org/10.5194/egusphere-2026-2723
Preprint. Discussion started: 13 July 2026

can account for the observed differences. Rather than seeking full mechanistic closure, this study aims to develop a framework to compare the κ values derived from different hygroscopicity determination approaches of the measured biomass-burning aerosol particles.

2 Method

2.1. Experimental Overview

The biomass burning (BB) study conducted in this study was part of a series of biomass burning experiments conducted at the University of Manchester in April and September 2022 (Chen et al., 2025; Oghama et al., 2026; Oghama et al., 2025; Evan et al., 2025; Evan et al., 2024). The experiments used the existing Manchester Aerosol Chamber (MAC, Shao et al. 2022), connected to a commercial wood-burning heating stove (Esse 175F; https://www.esse.com/heating-products/stoves/esse-175-f/), located outside the laboratory building, as the combustion source. The stove's catalytic filter compartment was removed for these experiments. A range of instruments was connected to the chamber, either directly or indirectly. The main instruments used in this study included Scanning Mobility Particle Sizer (SMPS), Hygroscopic Tandem Differential Mobility Analyzer (HTDMA), Cloud Condensation Nuclei Counter (CCNC), Aerosol Mass Spectrometer (AMS), and single particle soot photometer (SP2). These instruments were connected via a Nafion dryer to the MAC.

Figure 1 below illustrates the setup of the instruments used in this study. A complete schematic of the experimental setup for the April and September 2022 biomass burning (BB) campaigns at the project at UoM is being prepared in a separate manuscript. Generally, the dried, sampled chamber air containing biomass-burning smoke was split into two lines. The first line was passing air through an aerosol charger before entering both the HTDMA and CCNC instruments in parallel. The second line alternately passed air through either a heated thermodenuder line or a bypass line. The output was then analysed in parallel using the SMPS, SP2, and AMS instruments. During the last 2-3 hours of the experiment, a programmed thermodenuder heating cycle was run. Data points at which the thermodenuder was on during the cycles were excluded from the whole dataset, then the remaining data was saved as the non-thermodenuded data – the dataset used in the current study. Meanwhile, the excluded data was saved as the thermodenuded dataset for volatility investigation, not discussed here.

https://doi.org/10.5194/egusphere-2026-2723
Preprint. Discussion started: 13 July 2026

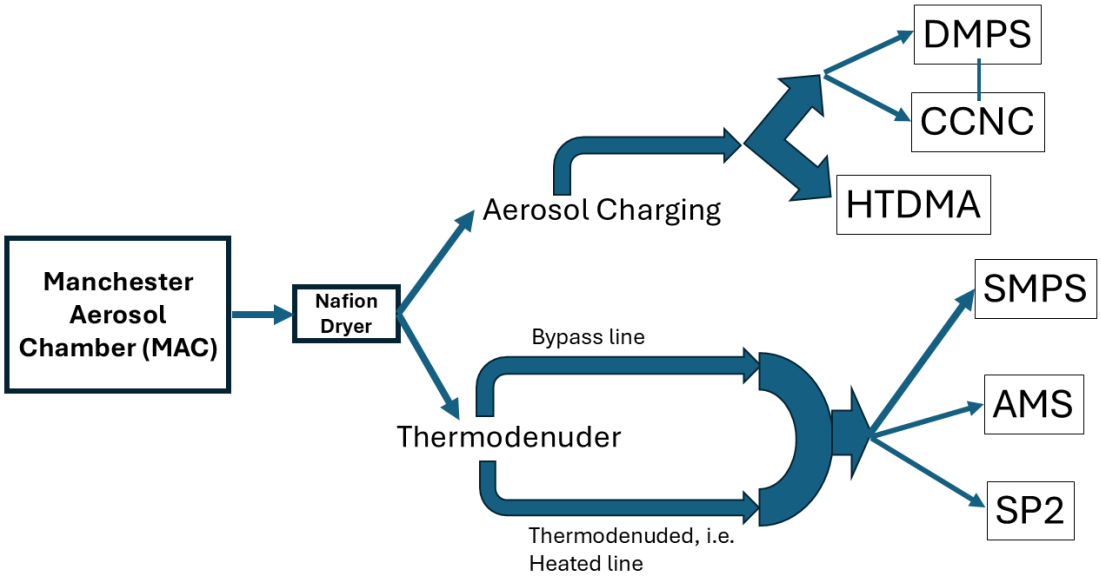

Figure 1: Schematic of the instrument setup showing the transfer of smoke samples from the Manchester Aerosol Chamber (MAC) to downstream measurement instruments used in the current study

On each experiment date, smoke emission was generated by burning fuel inside the stove using outdoor ambient, non-filtered air. The emissions were subsampled from a 125mm in diameter port located at the exhaust stack. This was combined with the first-stage dilution using compressed air coming from inside the laboratory, controlled by a mass flow controller (MFC). The purpose of this first-stage dilution was to prevent water condensation caused by cooling. This first-stage diluted smoke was drawn using a modified ejector diluter (Dekati® eDiluter™ Pro), bypassing the dilution to act solely as an injection unit into the MAC. At the start of the smoke injection process, the chamber was pre-filled with filtered, compressed dry air to approximately one-third of its volume. Smoke was injected continuously while the chamber was intermittently filled with compressed dry air. This approach was carefully adjusted to roughly achieve the targeted initial total particle mass concentration at the start of the experiment.

Two types of burning phases were tested: smouldering and flaming, for both softwood and hardwood. For peat and leaves, only smouldering-type smoke was tested. For all experiments, fuel burning was preceded by heating the stove, which in turn facilitated combustion. This was done by igniting wood kindling. Once the stove and smoke injection system were ready, with no unburnt ignition materials or smoke remaining in the stove, a piece (or pieces) of the fuel to be examined was added and burned. The stove door was then closed, while the stove ventilation was left open. The tests comparing smouldering versus flaming of the same fuel type were done on a different experimental day. On a flaming experiment day, the smoke produced while the fire was still visible was sampled, diluted, and injected into the chamber. On the smouldering experiment day, specifically for the wood-type fuels, the stove ventilation was closed after the initial burning of the wood sample to deplete

https://doi.org/10.5194/egusphere-2026-2723
Preprint. Discussion started: 13 July 2026

oxygen and extinguish the flame. Once the flame was no longer visible, but smoke was still being produced, the smoke was sampled, diluted, and injected into the chamber as smouldering smoke. Leaf and peat burning followed procedures similar to those of the wood-type smouldering experiment.

2.2. Hygroscopic Tandem Differential Mobility Analyser (HTDMA) measurements

HTDMA was used to observe hygroscopicity behaviour of submicron particles at sub-saturated humidity. The HTDMA used in this research was a custom-built system manufactured by University of Manchester (Wang et al., 2022; Good et al., 2010a). The system consisted of a series of components: a first DMA, a humidifier, a second DMA, and a water-based CPC, all connected in sequence. In each measurement, the first DMA selects a monodisperse particle size from the incoming flow of dried and charged biomass-burning smoke aerosol particles based on the set and connected controlling PC program. These particles then pass through the humidifier, which in this study was set to 90% RH. The humidified particles flow into the second DMA, coupled with the CPC, to measure the size distribution of the humidified particles.

The growth factor (GF) values are plotted on the x-axis, where GF is calculated by dividing the measured second DMA size (Dp_i) by the initial particle size (Dp_0) from the first DMA ($GF = Dp_i/Dp_0$). In this study, the second DMA scans 24 steps, with selected GF ranging from 0.75 to 2.6. This means the second DMA selects 24 particle sizes around the selected initial size to match the set measured GF values. The settling time for each step was 10 s, followed by 10 s of CPC reading time. Therefore, each complete scan took 8 minutes. Several dry particle sizes were selected and tested in this study for each loop of measurements.

Throughout each experimental campaign (April and September 2022), the HTDMA system underwent two calibrations: one at the start and one in the middle of the campaign. The calibrations included both DMA size calibration and humidity calibration. The DMA size calibration was performed using monodisperse polystyrene latex (PSL) particles with known sizes, as indicated on the manufacturer's PSL solution bottle label. The humidity calibration, which included both dry and wet conditions, was done using a nebulized solution of ammonium sulfate, a compound with well-known hygroscopicity behavior.

2.3. CCNC (CCN counter) measurements

CCNC was used to observe water affinity behavior of submicron particles under supersaturation conditions, specifically to assess the ability of the particles to be activated as cloud droplets. The CCNC measurements in this research were conducted by coupling a commercial CCNC system, manufactured by Droplet Measurement Technologies (DMT) (Wang et al., 2022; Roberts and Nenes, 2005), with a differential mobility particle system (DMPS) system consisting of a DMA (type: Finnish Vienna Long) and a butanol-based CPC model 3775. Similar to the HTDMA system, the aerosol particles were flowed through

https://doi.org/10.5194/egusphere-2026-2723
Preprint. Discussion started: 13 July 2026

a Nafion dryer, then through an aerosol charging before entering either the DMPS system or the CCN counter (CCNC) system. The sheath air flow in the CCNC was set to 3 L/min, while the aerosol flow was 0.3 L/min.

CCNC measurements in this study were performed in size-scanning mode rather than supersaturation scan mode, tested at five supersaturation levels in sequence. The set values were 0.1%, 0.2%, 0.3%, 0.4%, 0.5%. The starting dry particle size (Dp) measured in the DMPS system was 20 nm or as low as possible, but with a voltage not less than 50 V. The final scanning Dp was 517 nm, or as large as possible, while ensuring the total scan time did not exceed 600s (10 minutes). A loop of the full CCNC size-scanning was started from the lowest supersaturation level until the highest level, then an additional 10-minute measurement at the lowest supersaturation was performed at the beginning of the new cycle for stabilization purposes, so six full size scans in a cycle. In each scan, a size-resolved particle activation ratio (SPAR) dataset will result from the parallel measurements of initial particle concentration by CPC, and activated particles by CCNC for each scanned dry particle size, Dp.

As with the HTDMA system, the calibration of the DMPS-CCNC coupling was conducted using PSL particles and ammonium sulphate. The PSL were used to calibrate the DMA particle sizes, and the ammonium sulphate solution was used to calibrate the CCNC. The pair of D50 values as the Dp values and the tested SS values as the critical SS values were compared to the reference values to ensure accuracy (Good et al., 2010; Rose et al., 2008; Irwin et al., 2010). The SS calibration results in this study showed corrected tested SS values of 0.1%, 0.3%, 0.5-0.6%, 0.8%, and 1%.

2.4. AMS measurements

The composition and mass of nonrefractory aerosols were analyzed using a high-resolution time-of-flight aerosol mass spectrometer (CR-ToF-AMS, ARI Inc., USA; Drewnick et al., 2005) with a sampling rate of 0.1 L/min. The AMS collects submicron particles in the aerodynamic diameter range of ~50–800nm via an aerodynamic lens. Regular calibrations of the AMS were performed following procedures established by Jimenez et al., (2003) and Allan et al., (2004). During the experimental campaign, a series of calibrations was conducted using monodisperse ammonium nitrate and sulfate particles (350 nm). The average ionization efficiency of ammonium nitrate was determined to be 5.2×10^{-7} (6.08×10^{-7}; 4.32×10^{-7}) (April); 4.535×10^{-7} (4.82×10^{-7};4.25×10^{-7}) ions/molecule (September). Meanwhile, specific relative ionization efficiencies (RIEs) were established for $NH4^{+}$ and $SO4^{2}$ as 4.3556 and 1.0888, respectively, through ion balance assessments of ammonium nitrate and ammonium sulfate in these calibrations. Default value of 1.4 was set for the RIEs of all organic compounds (Alfarra et al., 2004).

2.5. SP2 measurements

https://doi.org/10.5194/egusphere-2026-2723
Preprint. Discussion started: 13 July 2026

A Droplet Measurement Technologies SP2 was used to measure both concentrations and mixing state of refractory BC within particles. The measurement range for the BC-containing particles was 70-850 nm equivalent spherical diameter. (Mori, T., et al., 2014). The SP2 measurement is based on the incandescence mechanism, where the refractory BC mass within a particle is proportional to the intensity of the incandescence signal detected by the SP2. When a BC-containing particle passes through an intra-cavity Nd:YAG laser beam (at λ = 1064 nm), the BC absorbs the laser energy and heats up. As the temperature increases, the BC emits visible light upon reaching its boiling point and incandesces. The mass of BC is then converted to a spherical equivalent BC core diameter (DC) using an assumed density of 1.8 g cm^{-3}.

The SP2 also provides information on the mixing state and/or the coating of BC-containing particles by measuring the light-scattering signal at λ = 1064 nm. This signal is processed using a method called the leading edge only (LEO) technique, as detailed in previous studies (Liu et al., 2017; Taylor et al., 2015; Gao et al., 2007). Briefly, the LEO method reconstructs the distorted scattering signal when the BC-containing particle loses its coating caused by the laser heating as it passes through the laser beam (Gao et al., 2007). The SP2 incandescence signal was calibrated following the procedure outlined in Laborde et al., (2012), using Aquadag BC particle standards. Calibration of the scattering channel was done using polystyrene latex spheres (PSLs) with a particle size of 300 nm. To interpret both the diameter of the BC-containing particles (DP) and shell-to-core ratios (DP/DC), a Mie core-shell model was employed (Taylor et al., 2015).

2.6. Data Selection and Processing

The data processing aimed to use all available data generated by the instruments during each experiment date in the campaign. Data was analysed for all experiments for which both HTDMA and CCNC instruments were available. The selection of AMS and SP2 data for chemical-based hygroscopicity predictions was based on the dates corresponding to either HTDMA or CCNC datasets. Because HTDMA and CCNC measurements were not available at identical time points across all experiments, two slightly different prediction datasets were constructed. For each instrument, the prediction data were subset to include only time points for which concurrent HTDMA or CCNC measurements existed, ensuring one-to-one temporal correspondence in the comparisons. If a necessary component dataset for the prediction, such as SP2 data, was unavailable for a specific date, neither the CCNC nor HTDMA datasets on that date were used. Table S1, Table S2, and Table S3 show the selected datasets for HTDMA-measured versus predicted hygroscopicity values, CCNC-measured versus predicted hygroscopicity values, and HTDMA versus CCNC values, respectively.

HTDMA data processing was done using the HTDMA IGOR toolkit (Gysel et al., 2009). The growth factor (GF) curve was fitted with a piecewise linear algorithm, which corrects for DMA broadening (Xu et al., 2021). This method, introduced by Gysel et al., (2009) was implemented with a bin of 0.1 for all datasets in this study.

https://doi.org/10.5194/egusphere-2026-2723
Preprint. Discussion started: 13 July 2026

The raw data from the CCNC instrument were processed using the IGOR CCNC toolkit, generating the size-resolved particle activation ratio (SPAR). Among three existing parameterization schemes, the method by Rose et al., (2008) was recommended due to its wide use and consistency with other models (Rose et al., 2008; Tao et al., 2024). This study employed an improved logistic model in MATLAB for curve fitting, defined as:

$$y = \frac{a}{(1 + exp\left(-b * (x - c)\right))}$$

where "a" value represents the maximum activation fraction (MAF), "b" value is the 1/asymptote, and "c" is the D50, the activation diameter at which 50% of particles are active or commonly known as Da, i.e. activation diameter. This formula is equivalent to one of the SPAR formulas proposed by Deng et al (2013):

$$\text{AR } (D_p) = \frac{MAF}{(1+exp\,(\frac{Da-Dp}{\sigma}))} \quad ,$$

$AR(D_p)$ means Activation ratio at a certain dry particle size (D_p). Parameters derived from curve fitting were saved, and the D50 values were input back into the CCNC IGOR toolkit to calculate CCNC κ values. MATLAB was chosen for practical reasons, allowing for easier comparison of fitted curves across time points by overlapping graphs.

The following Kohler model equation was used to derive the relationship between particle size, hygroscopicity, and water activity:

$$s = \frac{D_{wet}^3 - D_s^3}{D_{wet}^3 - D_s^3\,(1-\kappa)}\; exp\; exp\,(\frac{4\sigma_{sol}\,M_w}{R\,T\,\rho_{.w}D_{wet}})$$ (Rose et al., 2008).

This model, highlighted by Rose et al. (2008), was applied to ammonium sulfate calibrations for the CCNC instrument. For accurate results, hygroscopicity predictions for inorganic salts such as NaCl and $Na_2(SO_4)$ relied on water activity from the Aerosol Inorganics Model (AIM) or similar models, ensuring high accuracy.

The chemical composition-based κ prediction was calculated as follows:

$$\kappa = \kappa_{Org}\; x\; f_{Org} + \;\kappa_{inorg}\; x\; f_{inorg} + \;\kappa_{BC}\; x\; f_{BC}$$

at which κ_{Org} is the organic κ; κ_{inor} is inorganic κ; and κ_{BC} is black carbon (BC) κ; Meanwhile, f_{Org} is the organic mass fraction and f_{inorg} is the inorganic mass fraction. By using data from AMS and SP2 instruments for the κ prediction calculation, the following equation was used:

$$\kappa = 0.1 \text{ x } \frac{AMS\ Organic}{AMS\ Organic+AMS\ NH4+AMS\ SO4+AMS\ NO3+AMS\ Chl+SP2\ Black\ Carbon} +$$

$$0.6 \text{ x } \frac{AMS\ NH4+AMS\ SO4+AMS\ NO3+AMS\ Chl}{AMS\ Organic+AMS\ NH4+AMS\ SO4+AMS\ NO3+AMS\ Chl+SP2\ Black\ Carbon}$$

https://doi.org/10.5194/egusphere-2026-2723
Preprint. Discussion started: 13 July 2026

The base case fractional κ values were selected as 0.1, 0.6, and 0 for the organic fraction, inorganic fraction, and BC, respectively. Those selected values follow widely adopted conventions in κ-Köhler-based CCN closure studies (Petters and Kreidenweis, 2007). The inorganic κ reflects the typical hygroscopicity of atmospherically relevant ammonium sulfate–nitrate mixtures (Dusek et al., 2006; Gunthe et al., 2009), while κ_{org} = 0.1 represents a central value commonly reported for fresh to moderately aged biomass-burning organic aerosol in both laboratory and field studies (Petters et al., 2009; Carrico et al., 2010; Lambe et al., 2011; Engelhart et al., 2012). Black carbon was treated as non-hygroscopic (κ = 0), consistent with κ-Köhler theory and previous CCN studies of soot and BC-containing particles (Petters and Kreidenweis, 2007; Rose et al., 2010; Kuwata et al., 2009).

Due to differences in instrument time resolution, all datasets were averaged to hourly time intervals before inter-method comparison. The final datasets consisted of size-number-weighted hourly mean HTDMA-derived κ, hourly mean CCNC-derived κ at each supersaturation level, and hourly mean AMS–SP2 composition-based predicted κ. Uncertainties shown as error bars represent propagated uncertainties associated with the corresponding averaging and retrieval procedures: HTDMA retrieval and size-number-weighted averaging, CCNC activation-curve fitting and hourly averaging, and AMS–SP2 component mass propagation through the composition-based prediction. Error propagation was performed according to the applied averaging process or methods. Detailed description of both the averaging process and the corresponding error propagation was in the Supplementary Information, Notes. S1, Fig. S1., and Fig. S2.

To address uncertainty in the components' fractional κ (organic, inorganic, or black carbon) values, additional examination was conducted using a range of fractional κ values: BC κ = -0.05, inorganic κ = 0.4, organic κ = 0.05 for the minimum values, and BC κ = 0, inorganic κ = 0.8, organic κ = 0.15 for the maximum values. The range included negative values for BC κ to account for possible shrinkage of the BC core due to restructuring and compaction from an aggregate to a more spherical form with reduced mobility size under humid conditions. This phenomenon is influenced by the coating state of BC (e.g., uncoated, partially coated, or fully coated), as illustrated by He et al. (2019) and Zhang, X., & Mao, M. (2019). The examination results for the two sets of component κ values, i.e., the minimum and maximum sets, were presented with new error bars representing the resulting minimum and maximum κ values, replacing the propagated values in the base case. By applying the extended fractional κ values, the prediction of κ values was evaluated across a range of potential component κ values.

Although the ZSR κ mixing rule is formally defined using component volume fractions under the internally mixed assumption (Petters and Kreidenweis, 2007), mass fractions were employed in this study as a practical approximation. This choice was made because the AMS and SP2 instruments provide direct mass-based measurements of organic, inorganic, and refractory black carbon, whereas comprehensive size-resolved density data for all aerosol components were unavailable. Similar mass-fraction-based approximations have been adopted as first-order approaches when component densities are expected to be

https://doi.org/10.5194/egusphere-2026-2723
Preprint. Discussion started: 13 July 2026

broadly comparable or when organic material dominates aerosol mass (Gunthe et al., 2009; Pöhlker et al., 2023). The implications of this approximation, particularly in the current biomass burning study, are discussed in the limitations section.

3. Results and Discussion

As described in **Sec. 2**, among several approaches previously used in calculating chemical composition-based κ predictions, as summarized in Table S4 and explained in Note S2, this study calculated the chemical composition-based κ prediction based on mass fractions, instead of volume fractions, with BC treated as a separate fraction alongside inorganic and organic fractions. Despite the potential added bias in the resulting absolute κ values caused by limitations of the applied assumptions, which will be discussed in the **Sec. 3.5.8**, the mass fraction-based predicted κ calculation should still remain useful for identifying general fuel- and burn-phase-dependent behavior and for comparing the direction of composition-based predictions relative to direct HTDMA- and CCNC-derived κ values.

3.1. HTDMA Measurement and Prediction Results

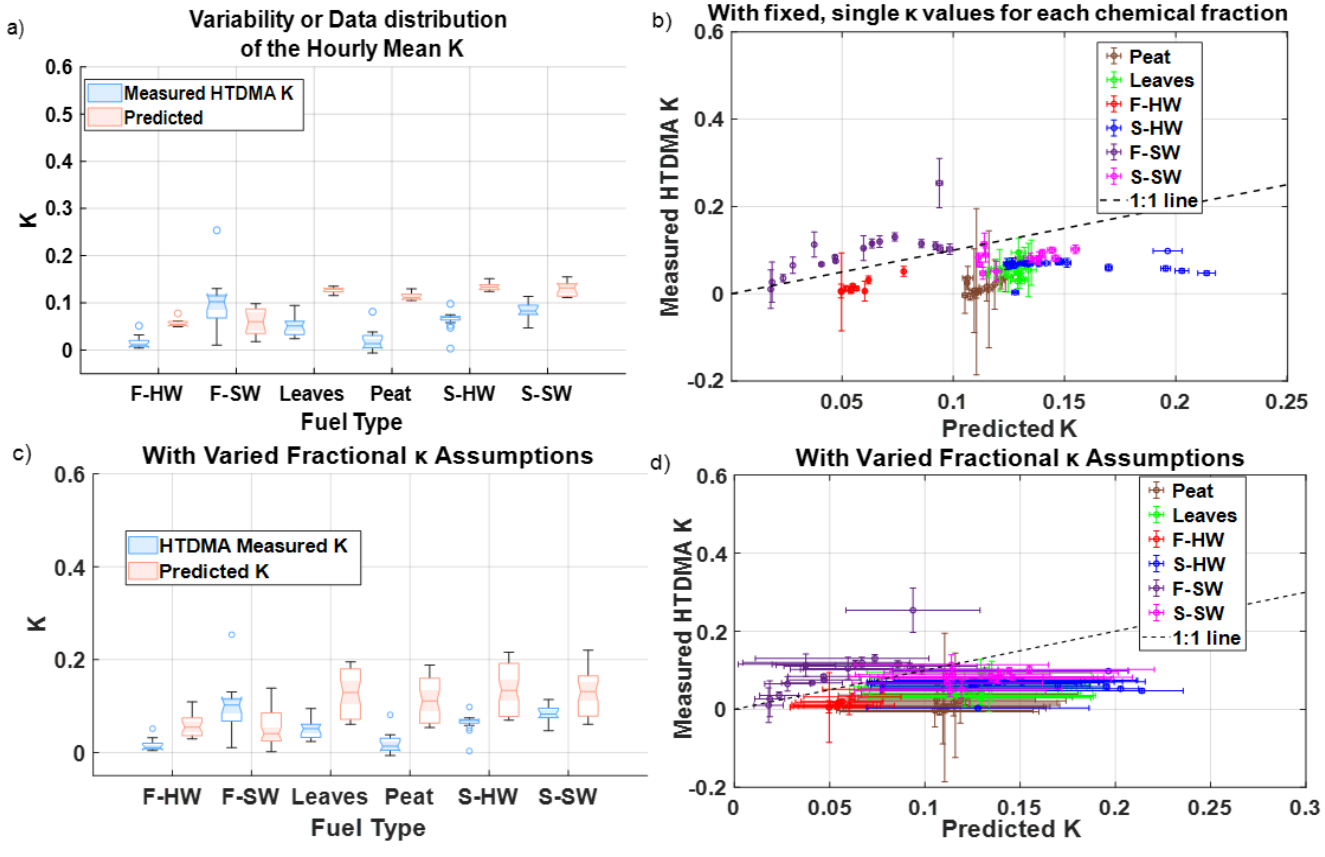

https://doi.org/10.5194/egusphere-2026-2723
Preprint. Discussion started: 13 July 2026

Figure 2. Data distribution comparisons of each experiment type between the hourly averaged HTDMA-measured size-number-weighted mean κ values and hourly averaged chemical composition-based predicted κ values, collected from all repetitions and all hourly fresh-aging stage period intervals (**a, c**), and hourly averaged data points of HTDMA-measured size-number-weighted mean κ values **versus** chemical composition-based predicted κ values, along with their propagated error bars, collected from all repetitions and all hourly fresh-aging stage period intervals (**b, d**). ***Further note:*** *Top panel* (**a, b**) Fixed, single values of each chemical fraction, i.e., organic κ value of 0.1 and inorganic κ value of 0.6 were used for predictions with horizontal error bars in **b**) showing propagated errors from the instruments data; *Bottom panel* (**c, d)** Varied fractional κ value assumptions were used for the predictions, with horizontal error bars in **d**) showing minimum and maximum κ values resulting from the use of minimum and maximum fractional κ values, respectively. HTDMA-measured κ error bars, i.e., the vertical error bars, in both **b**) and **d**) reflect error propagation between the instrumental curve fitting errors, within-hour variability, and across-size variability. Different data points can come from different repetitions, different 1-hour intervals, or both. Further explanation about this graph is in the Supplementary Information, Notes S3.

Figure 2.a) and Fig. 2.b) show that all predictions using organic κ of 0.1 and inorganic κ of 0.6, except for those for flaming softwood, overestimated the HTDMA-derived κ values. **Figure 2.a)** shows that discrepancies between measured and predicted κ values varied across experiment types. The predicted κ values were distinctly separated by burning types: less than 0.1 for flaming experiments and greater than 0.1 for smouldering experiments, with no overlapping error bars (**Fig 2.b)**. Additionally, the absence of overlapping notches between smouldering and flaming experiments indicates that the medians of predicted κ values between these two burning phases differed significantly at the 95% confidence level, as shown in **Fig 2.a).** On the other hand, HTDMA measurements showed no clear separation between the different burning types. Further discussion regarding the more detailed patterns of the HTDMA-derived κ values, along with investigation of some observed outliers and large propagated error bars, is in the Supplementary Information, Notes S4 and Fig. S5.

In **Fig. 2.b**, some measured HTDMA κ values started to align with the predicted κ range after applying the plausible range of fractional, i.e., component κ values' sensitivity exploration, while others still exhibited significant discrepancies. Furthermore, only a few cases showed overlapping notches in the box-and-whisker plot of HTDMA-measured κ and predicted κ hourly mean values, indicating that most of these two datasets were still significantly different. A table summarizing the predicted-to-HTDMA measured ratio was in SI. Table S5. Based on the table, all HTDMA-measured values are well below the predicted values, except for flaming softwood. In this subsection, significant differences remain after considering some potential factors influencing discrepancies between the HTDMA κ values measurement and AMS-SP2 predictions of κ values discussed: 1) the too-narrow single choice of representing component κ values - addressed by a wider range of component κ values, and 2) the possible BC restructuring - addressed by adding a negative BC κ value. Other possible factors were analyzed in **Sec. 3.5**.

https://doi.org/10.5194/egusphere-2026-2723
Preprint. Discussion started: 13 July 2026

3.2. CCNC Measurement Versus Prediction Results

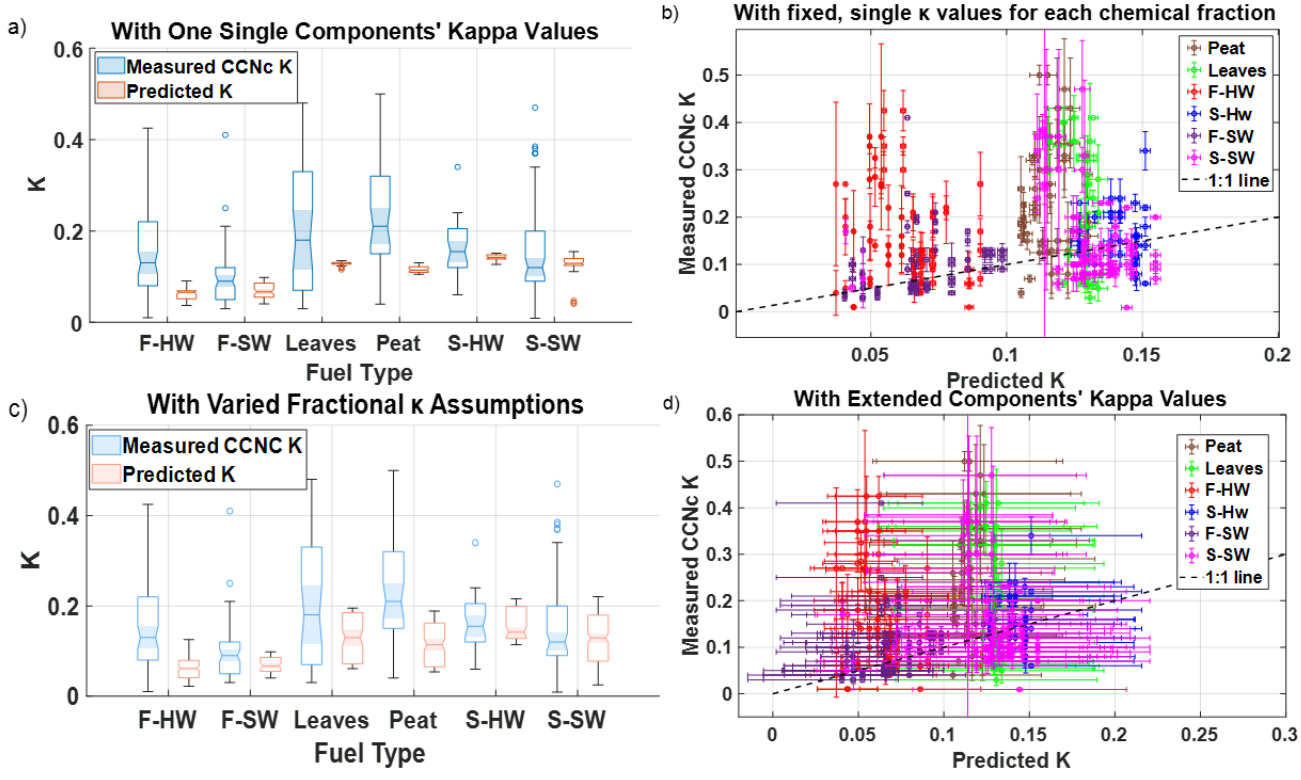

Figure 3. Data distribution comparisons of each experiment type between the hourly averaged CCNC-measured mean κ values and hourly averaged chemical composition-based predicted κ values, collected from all repetitions, all tested Supersaturation (SS) values, and all hourly fresh-aging stage period intervals (**a, c**), and hourly averaged **data points** of CCNC-measured mean κ values **versus** chemical composition-based predicted κ values, along with their propagated error bars, collected from all repetitions, all tested Supersaturation (SS) values, and all hourly fresh-aging stage period intervals (**b, d**). ***Further note:*** *Top panel* (**a**) Fixed, single values of each chemical fraction, i.e., organic κ value of 0.1 and inorganic κ value of 0.6 were used for predictions with horizontal error bars in **b**) showing propagated errors from the instruments data; *Bottom panel* **(c, d)** Varied fractional κ value assumptions were used for the predictions, with horizontal error bars in **d**) showing minimum and maximum κ values resulting from the use of minimum and maximum fractional κ values, respectively. CCNC-measured κ error bars, i.e., the vertical error bars, in both **b**) and **d**), reflect error propagation between the instrumental curve fitting errors and within-hour variability. Data from different tested SS values were treated as different data points, i.e., not averaged. Therefore, different data points can come from different repetitions, different 1-hour intervals, different tested SS, or a combination of any of these.

https://doi.org/10.5194/egusphere-2026-2723
Preprint. Discussion started: 13 July 2026

Figure 3.a) shows the data distribution of hourly mean CCNC-measured κ values at all tested Supersaturation (SS) values and all time intervals for each experiment type, compared with the corresponding mean predicted κ values distribution. Meanwhile, **Fig. 3.b)** shows exactly the data points of them and includes the propagated error bars for each of the hourly mean data points. As the HTDMA data, the CCNC data points were also collected across multiple repetitions and aging stages, including dark aging and pre-aging, representing fresh emission. However, the CCNC data were tested at several supersaturation values. The data points were aggregated across all tested supersaturation values. The supersaturation-separated version of **Fig.3.a** was provided in Fig. S6. Meanwhile, examples of the time series plots for each supersaturation level are shown in Fig. S4.

Unlike HTDMA measurements, almost all CCNC-measured κ values were underestimated by the chemical composition-based prediction. The exception is the smouldering softwood experiments, whose CCNC κ median is lowest among smouldering experiments. Other experiment types have higher CCNC-derived median κ than the corresponding median predicted κ. The CCNC-derived κ versus predicted-κ discrepancies were either significant, as in the Peat and Flaming-Hardwood experiments, or overlapping in some areas, as in the rest of the experiment types. The width of the CCNC-measured κ distribution varied significantly across experiment types, with some outliers and differing values. The large difference between HTDMA and CCNC measurements was not due to minor differences in the availability of data points. This was shown by similar values of the predicted κ values across the HTDMA vs. the prediction dataset and CCNC vs. the prediction dataset, whose selections of the experiment dates and hourly time intervals of the predicted κ dataset followed the corresponding instrument being investigated (HTDMA or CCNC).

Figure 3.b) underscores that some of the experiments had larger propagated errors in CCNC-measured κ values compared to the propagated error of the predicted values, while other experiments had much smaller errors. As mentioned before, graphs separating at distinct supersaturation values are shown in Fig. S6. The variability of the hourly mean CCNC-measured κ values showed significant dependence on the SS applied during the measurements. The error bars reflected how well the sigmoid curve fit the measured data, accounting for the one-hour variability in the propagation process. Instrumental measurement uncertainty, such as the relative deviation of less than 10% for SS > 0.1%, was reported by Rose et al. (2008). However, that kind of uncertainty was not accommodated in the current error propagation in this study. That SS-dependent instrumental uncertainty seemed to be a relatively minor contribution compared to other sources of variability, such as the curve fitting-derived uncertainty in the resulting D50 values themselves, and is unlikely to affect the calculated propagated errors substantially.

A table summarizing the predicted-to-CCNC measured ratio was in Supplementary Information, Table S6. Based on the table, most (but not all) of the CCNC-measured values were underestimated by the prediction, i.e., the predicted-to-measured ratio was less than 1. Meanwhile, the overpredicted values are not too far from the ratio of 1, i.e., about 2 as the maximum (in contrast to massive predicted-to-HTDMA measured κ values ratio). The higher predicted-to-measured mean κ values ratio

https://doi.org/10.5194/egusphere-2026-2723
Preprint. Discussion started: 13 July 2026

occurred for Leaves at SS=0.5-0.6%; Smouldering-Hardwood at SS=0.8% and 1%; and Smouldering-Softwood at SS=0.3%; SS=0.5-0.6%; SS=1% (at all tested SS, except SS=0.1%).

3.3. CCNC VS HTDMA Measurements

Across all fuels and aging conditions, CCNC-derived κ values were systematically higher than HTDMA-derived κ values, except for data points near the 1:1 line (**Fig. 4**). This indicates a strong regime-dependent hygroscopicity. Previous studies have reported higher CCN κ values than HTDMA κ values for organic-dominant particles (Jaatinen, A. et al., 2014; Wex, H. et al., 2009).

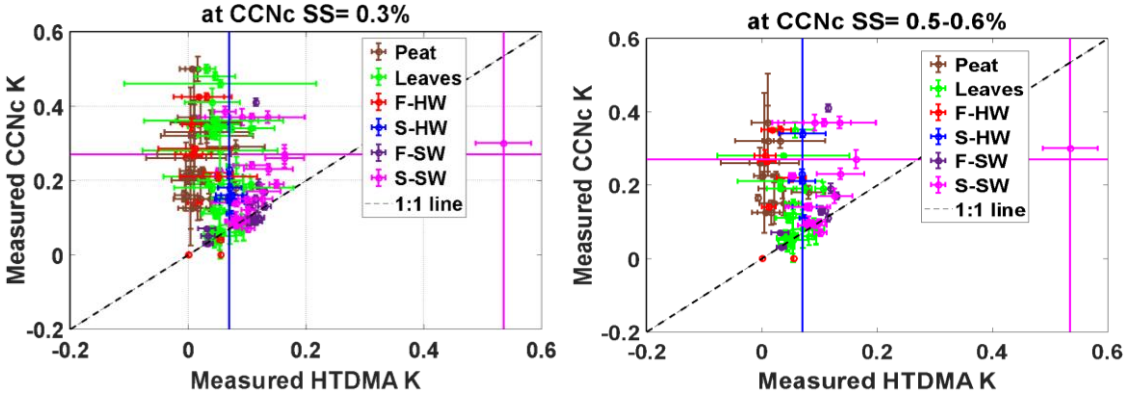

Figure 4. HTDMA vs CCNC measurement at SS=0.3% (a) and SS= 0.5-0.6% (b). The HTDMA κ values are the size-number weighted average hourly mean values with propagated errors. The CCNC κ values are the CCNC hourly-averaged κ values with propagated errors. Comparison of the median values of CCNC κ values versus HTDMA κ values for each experiment type can be seen in Fig. S13, where the median HTDMA κ value of flaming-softwood experiments is only slightly higher than that of CCNC κ, while other experiment types have significantly higher CCNC median κ values than HTDMA median κ values.

Tables S5 and S6 demonstrate the relative dependency of the HTDMA size effect and of the CCNC supersaturation effect on the experiment type - both fuel type and burning phase (Table S7). The magnitude of size-dependent κ variability derived from HTDMA measurements is substantially larger than the magnitude of supersaturation-dependent κ variability derived from CCNC measurements. In addition, the fuel-type dependence of the size effect is markedly stronger than that of the supersaturation effect.

3.4. Inter-method Comparison and Summary

https://doi.org/10.5194/egusphere-2026-2723
Preprint. Discussion started: 13 July 2026

Table 1 below summarizes the inter-method bias, Δκ (Predicted − Measured) of the median and mean values of each experiment type. The most consistent shift direction of the inter-method discrepancies was those between HTDMA and CCNC where CCNC κ values were higher than the corresponding HTDMA κ values. The highest gap between the κ values from those two instruments resulted from the peat experiments. The second and third highest gaps were from leaves and flaming-hardwood, respectively. Meanwhile, the fourth, fifth, and sixth largest gaps, respectively, were from smouldering-hardwood, flaming-softwood, and smouldering-softwood.

All the median and mean κ values obtained from HTDMA measurements were overpredicted, except in flaming-softwood experiments. Meanwhile, the median and mean CCNC κ values were underpredicted, except at smouldering-softwood experiment, which had only slightly higher predicted median κ value than the corresponding CCNC derived median κ value. Best predictions relative to CCN derived κ occurred in smouldering-softwood and smouldering-hardwood experiments, while the worst were in peat and flaming-hardwood experiments. Relative to HTDMA derived κ values, the best predictions were from smouldering-softwood experiments, while the worst predictions were from peat experiments.

Table 1. Inter-method bias of each experiment type. Positive Δκ indicates either overprediction (prediction > HTDMA or prediction > CCNC) or higher HTDMA κ than CCNC κ; negative values indicate either underprediction (prediction < HTDMA or prediction < CCNC) or lower HTDMA κ than CCNC κ.

Experiment Type	Δ (Prediction – HTDMA) κ, Median	Δ (Prediction – CCNC) κ, Median	Δ (HTDMA – CCNC) κ, Median	Δ (Prediction – HTDMA) κ, Mean	Δ (Prediction – CCNC) κ, Mean	Δ (HTDMA – CCNC) κ, Mean
Flaming Hardwood	+0.045	-0.070	-0.115	+0.020	-0.101	-0.121
Smouldering Hardwood	+0.069	-0.021	-0.090	+0.098	-0.016	-0.114
Flaming Softwood	-0.036	-0.023	-0.036	-0.020	-0.036	-0.018
Smouldering Softwood	+0.035	+0.008	-0.027	+0.005	-0.035	-0.040
Peat	+0.098	-0.098	-0.196	+0.092	-0.126	-0.218
Leaves	-0.036	-0.036	-0.115	+0.077	-0.104	-0.174

Based on the **Table** 1, within the same burning phase, the composition-based predicted κ values remain clustered more tightly (range = 0.069, ranging from 0.060 to 0.129, median values) across fuel types than the CCNC-derived κ values (range = 0.120, ranging from 0.090 to 0.210, median values). The latter retain pronounced fuel-specific variability in addition to their burn-phase dependence. Quantitatively, the magnitude of variability among CCNC-derived κ values across the six experiment types exceeds the average inter-method discrepancy of predicted κ values relative to measured CCNC κ values, which were only between -0.098 and +0.008. Across the majority of supersaturation conditions and experiment types, CCNC-derived κ values

https://doi.org/10.5194/egusphere-2026-2723
Preprint. Discussion started: 13 July 2026

exhibit a positive offset relative to chemical-composition-based predicted κ values. The exceptional reverse occurred in most of the smouldering softwood experiments and in some other experiment types at higher supersaturations (Supplementary Information, Table S6)

Among the HTDMA median κ values, the magnitude of the fuel-to-fuel variability relative to the measurement versus prediction inter-method discrepancies of each of experiment types differs across different burning phases. Within the smouldering phase, fuel-to-fuel variability of the HTDMA κ values is lower (**0.017**, ranging from 0.115 to 0.132, median values) than the relative position of the predicted median κ values from the HTDMA median κ, which were **+0.069, +0.035, +0.098,** and **-0.036** for smouldering-hardwood, smouldering-softwood, peat, and leaves, respectively. Within flaming phase, the fuel-to-fuel variability was around **0.052,** representing gap between HTDMA median κ values of flaming hardwood at 0.015 and flaming softwood at 0.067. This variability was slightly higher than the discrepancy of the HTDMA κ values of each of flaming experiments from the corresponding predicted κ values, which were **+0.045** and **-0.036** for flaming-hardwood and flaming-softwood, respectively.

Overall, based on the median and mean values, the HTDMA κ values generally maintained approximately consistent lower values than CCNC κ values, though with varied gaps or discrepancies across the different experiment types. **Table 2** below shows the median and mean κ values for each experiment type across the three approaches, ordered from highest to lowest.

Table 2. Ranking of median κ and mean κ values in each experiment type using the three different approaches

Experiment type	**Highest, Median**	**Middle, Median**	**Lowest, Median**	**Highest, Mean**	**Middle, Mean**	**Lowest, Mean**
Flaming-Hardwood	CCNC κ (0.130)	Predicted κ (0.060)	HTDMA κ (0.015)	CCNC κ (0.161)	Predicted κ (0.060)	HTDMA κ (0.040)
Smouldering-Hardwood	CCNC κ (0.155)	Predicted κ (0.132)	HTDMA κ (0.065)	CCNC κ (0.163)	Predicted κ (0.133)	HTDMA κ (0.049)
Flaming-Softwood	HTDMA κ (0.103)	CCNC κ (0.090)	Predicted κ (0.067)	CCNC κ (0.105)	HTDMA κ (0.087)	Predicted κ (0.068)
Smouldering-Softwood	Predicted κ (0.127)	CCNC κ (0.120)	HTDMA κ (0.093)	CCNC κ (0.163)	Predicted κ (0.128)	HTDMA κ (0.123)
Peat	CCNC κ (0.210)	Predicted κ (0.115)	HTDMA κ (0.014)	CCNC κ (0.238)	Predicted κ (0.114)	HTDMA κ (0.020)
Leaves	CCNC κ (0.165)	Predicted κ (0.129)	HTDMA κ (0.050)	CCNC κ (0.231)	Predicted κ (0.128)	HTDMA κ (0.057)

https://doi.org/10.5194/egusphere-2026-2723
Preprint. Discussion started: 13 July 2026

Based on the **Table 2** above, the order of the experiment types starting from highest to lowest median or mean κ values were different for different methods. Under CCNC measurements, the highest to lowest median κ values were those from peat, leaves, smouldering-hardwood, flaming-hardwood, smouldering-softwood and flaming-softwood, respectively; while the order for the CCNC derived mean κ values were peat, leaves, smouldering-hardwood, smouldering-softwood, flaming-hardwood, and flaming-softwood. Under the chemical composition-based prediction calculations, the order of the median κ values, starting from the highest to lowest are smouldering-hardwood, leaves, smouldering-softwood, peat, flaming-softwood, and flaming-hardwood; whereas the order of the mean κ values were smouldering-hardwood, smouldering-softwood, leaves, peat, flaming-softwood, and flaming-hardwood. Both CCNC measurements and chemical-composition based predictions put κ values from flaming experiments in the 2-3 lowest values. Under HTDMA measurements, the order of the median κ values from the highest to lowest values were flaming-softwood, smouldering-softwood, smouldering-hardwood, leaves, flaming-hardwood, and peat; whereas the order of the mean κ values from the highest to lowest were smouldering-hardwood, flaming-softwood, leaves, smouldering-hardwood, flaming-hardwood, and peat.

Table 3. Relative magnitude (0–100) of fuel-type dependency of HTDMA-size and CCNC-supersaturation effects; Normalisation definition: Fuel-type dependency magnitude is normalised to 100 by dividing each variability range by the maximum range observed across all fuels for the same effect.

Fuel type	HTDMA size-dependency range (max–min)	HTDMA fuel-dependency magnitude of the size effect (0–100)	CCNC SS-dependency range (max–min)	CCNC fuel-dependency magnitude of the supersaturation effect (0–100)
Peat	45.98	100	0.273	17
Leaves	2.01	4	1.58	100
Flaming hardwood	7.17	16	0.33	21
Smouldering hardwood	7.35	16	0.75	48
Flaming softwood	0.42	1	0.33	21
Smouldering softwood	0.19	0	1.18	75

Lastly, **Table 3** above provides insights into the size dependence of the HTDMA and the supersaturation dependence of the CCNC calculated from the size-resolved prediction-to-HTDMA measured κ ratio, and supersaturation separated prediction-

https://doi.org/10.5194/egusphere-2026-2723
Preprint. Discussion started: 13 July 2026

to-CCNC measured κ ratio, provided in Table S5 and Table S6 in Supplementary Information, respectively. Size-dependent κ variability derived from the HTDMA measurements exhibits both a larger magnitude and a substantially stronger fuel-type dependence than the supersaturation-dependent κ variability observed in CCNC measurements. Across the six experiment types, the highest size dependence of the measured HTDMA κ values occurred in peat, smouldering-hardwood, flaming-hardwood, leaves, flaming-softwood, and smouldering-softwood, respectively. Meanwhile, the highest supersaturation dependence occurred in leaves, smouldering-softwood, smouldering-hardwood, flaming-hardwood, flaming-softwood, and peat, respectively.

3.5. Investigation of the sources of discrepancy in κ

While the κ framework has been shown to provide consistent representations of hygroscopicity for well-defined organic and inorganic compounds (Petters and Kreidenweis, 2007), the present results demonstrate persistent discrepancies between κ values derived from CCNC, HTDMA, and composition-based prediction for complex biomass-burning aerosols under controlled conditions. Under the Zdanovskii–Stokes–Robinson (ZSR) analog mixing framework, the distribution of κ across experiment types is expected to follow the bulk chemical composition of the aerosol, with variations driven primarily by differences in organic and inorganic fractions associated with fuel type and burn phase, while non-hygroscopic black carbon contributes by reducing the overall effective hygroscopicity. The composition-based predicted κ values, therefore, provide a reference expectation for how hygroscopicity should be structured across the dataset. Comparison with κ derived from HTDMA and CCNC measurements allows assessment of whether subsaturated growth, supersaturated activation, and bulk composition provide consistent representations of aerosol hygroscopicity, or whether systematic divergence emerges between regimes.

Within a given burning phase (flaming or smouldering), different fuel types exhibit roughly similar bulk chemical mass fractions of the major aerosol components (Supplementary Information, Fig. S3). All the bulk flaming smoke particles have black carbon as the most dominant component, while the bulk smouldering particles have organic as the most dominant component. Additionally, smoke particles from flaming experiments have a higher bulk inorganic-to-organic ratio. All the obtained bulk chemical composition information, along with the mixing rule equation in sec., yields the prediction of the bulk hygroscopicity of the particles. Under both the ZSR mixing assumption and the uniform fractional κ values (κ_{org} and κ_{inorg}) assumptions, observed similarity in bulk chemical composition within the same burning phase should lead to comparable κ values, unless additional factors play a dominant role.

In this current study, both CCNC-derived κ and AMS–SP2 chemical-composition-based predicted κ values show a clear dependence on burning phase, especially among the same fuel type, with systematically lower κ values in flaming experiments, likely associated with higher black carbon content. Hardwood burnt under smouldering conditions consistently has higher

https://doi.org/10.5194/egusphere-2026-2723
Preprint. Discussion started: 13 July 2026

values of both CCNC κ and predicted κ than those of hardwood burnt under flaming conditions. Similarly, softwood burnt under smouldering conditions consistently has higher κ values for both CCNC-derived and chemical composition-based predictions than softwood burnt under flaming conditions. Across all the six experiment types, there is, however, a significant overlapping area of the CCNC κ values between flaming hardwood and smouldering softwood – an exceptional smouldering experiment that has a lower median CCNC κ value than its corresponding median predicted κ value.

The κ values derived from CCNC measurements are generally higher than those derived from HTDMA across most experiment types, with composition-based predictions typically lying between the two. This consistent directional offset suggests that the observed divergence is not random and motivates a systematic evaluation of potential contributing factors. The following subsections assess the extent to which key factors—including black carbon treatment, assumptions in organic hygroscopicity, and size representation along with the size dependence of hygroscopicity—can account for the observed discrepancies. **Table 4** below summarizes the investigated factors, their expected effects, and the extent to which they are supported by the present dataset. Table S9 and Table S10 in Supplementary Information provide summary of Factor-by-Factor Evaluation of HTDMA versus AMS-SP2 κ discrepancies and CCNC versus AMS-SP2 κ discrepancies, respectively. Supplementary Information, Note S7 provides some further explanation of the investigations and/or detailed/additional explanation of some contributing factors, including mainly the non-tested measurement regime dependent factors and the unknown direction systematic CCNC versus AMS-SP2 based prediction discrepancy causing factors referring to the varied choices of adjustments and parameters as explained in Supplementary Information, Notes S6.

Table 4. Classification of factor categories contributing to discrepancies among κ values derived from HTDMA, CCNC, and AMS–SP2 approaches in the current biomass burning smoke study

No	Factor category	Primary nature	Suspected Direction			Investigated in this study	Investigation results (Validity Level of the Factor's Influence Presence)	Quantitatively Checked
			HTDMA	CCNC	AMS-SP2			
1	**Particle size representation** (number- vs mass-weighted for HTDMA versus AMS-SP2; number weighted D_{50} vs mass mean for CCNC versus AMS-SP2) combined with **Size-dependent hygroscopicity**	Combined Methodological / Systematic and Physicochemical	Depend on the particle size distribution nature, the selected particle sizes, and both direction and magnitude of the size dependence presence in the particles' hygroscopicity			Yes **Sect. 3.5.2** until **Sect. 3.5.4** Table S12.	Highly Valid	Yes (HTDMA only);
2	Organic hygroscopicity (κ_{org}) variability	Chemical	Depend on the actual κ_{org} of the particles relative to the current/initially used uniform κ_{org} value of 0.1			Yes **Sect. 3.5.6** Table S14.	Less valid (Could be improved with a bit more accurate investigation	Yes; .

https://doi.org/10.5194/egusphere-2026-2723
Preprint. Discussion started: 13 July 2026

							using directly measured O:C ratio values while determining the κ_{org} values and/or using the point-to-point κ_{org} value adjustment instead of mean-to-point adjustment)	
3	Number-weighted vs mass-weighted κ averaging	Methodological (HTDMA measurement)	Depends on the size dependence presence in the hygroscopicity of the bulk particles	Not applicable	Not applicable	Yes **Sect. 3.5.2** until **Sect. 3.5.4** Table S13	Less Valid (Could be improved with more accurate investigation using more accurate particle mass distribution instead of using SMPS- derived mass distribution that applied an assumed constant & uniform density)	Yes
4	External mixing (multiple hygroscopic modes; pure non-hygroscopic fraction presence)	Combined Methodological / Systematic and Physicochemical	Depend on the particle size distribution nature, the selected particle sizes, and both direction and magnitude of multiple hygroscopicity external mixing among the bulk particles.			Yes **Sect. 3.5.1** Table S11	***External mixing of non-hygroscopic/non-coated pure BC particles:*** Valid ***<u>Other external mixing:</u>*** Not systematically investigated, except the bulk size dependent hygroscopicity of the HTDMA κ values as in Factor number 1 investigation.	No
5	Condensable organic gases (co-/re-condensation during measurement)	Physicochemical (gas–particle partitioning) + kinetic / measurement-timescale dependent	Increase	Not applicable; OR Limited	Not applicable	No	Not investigated	No
6	Surface-active organic compounds (SVOCs / low-volatility organics)	Physicochemical; Regime dependent	Decrease or no effect	Mostly increase	Not applicable	No	Not investigated. Surface-active presence was only guessed through the high presence of	No

https://doi.org/10.5194/egusphere-2026-2723
Preprint. Discussion started: 13 July 2026

7	Particle phase state (viscosity / solidity)	Physical; Regime dependent	Decrease	No effect	Not applicable	No	Not investigated	No
8	Particle shape / restructuring / compaction	Physical	Decrease	Not affected	Not Applicable	No	Not investigated	No
9	Volume- vs mass-fraction use in ZSR mixing	Combined Methodological / Systematic and Physicochemical (AMS-SP2 based prediction related only)	Not Applicable	Not Applicable	Not known	No	Not investigated	No
10	Data processing / parameterization choices (SPAR fitting adjustment, chosen Köhler model, used minimum SSeff, chosen parameterization scheme, and choice to use an improved parameterization scheme for bulk particles that contain both hygroscopic particles with small sizes and nearly hydrophobic particles):	Systematic (CCNC measurement related only)	Not Applicable	Not known	Not Applicable	No (Just selected consistently) (Notes S6; Notes S7.2)	Not investigated	No

3.5.1 Role of black carbon presence and treatment

Based on the CCNC's size-resolved particle activation ratio (SPAR) curve sigmoid fitting, certain fraction of externally mixed non- hygroscopic particles was likely to be present (Supplementary Information, Fig. S11 and Fig. S12). The maximum values of the activation fraction in the CCNC sigmoid fitted SPAR curve both never reach the value of one and were lower than the maximum activation fraction of pure ammonium sulphate particles in the calibration measurements. The additional features of decreasing activation fraction (AF) after reaching its maximum AF values, i.e., small AF at large particle sizes is observed in the Fig. S11 and S12. This was also observed in the SPAR curves of inorganic particles externally mixed with combustion aerosol particles consisting of black carbon (Vu, D., et al 2019). On the other side, two peaks of hygroscopicity with the first hygroscopicity showing a growth factor (GF) value at around one in some HTDMA measurements observed indicating the likelihood of externally mixed nonhygroscopic particles. (Supplementary Information, Fig. S13, flaming-hardwood, 165 nm). A strong candidate of the nonhygroscopic fraction particles among the biomass burning smoke particles especially in the current study was black carbon (BC).

As the nature of the CCNC data processing when fitting a sigmoid curve to the recorded SPAR curve, the non-hygroscopic fraction was not considered in the determination of the bulk CCNC κ values of the whole population of the particles. The

https://doi.org/10.5194/egusphere-2026-2723
Preprint. Discussion started: 13 July 2026

exclusion of the non-activating fraction – likely suspected as the non externally mixed black carbon, would probably be initially expected to be the positive shifts' contributor of the CCNC κ values from the predicted κ values under flaming conditions, at which black carbon mass fractions are typically higher. Drawing the sigmoid curve only on the active population should inflate the κ values relative to bulk chemical κ values. How the SPAR curves were fitted and adjusted in this current study is detailed in Supplementary Information, Note S5-S6.

Contrary to this expectation, the present dataset shows no clear burn-phase driven pattern in the CCNC–AMS κ discrepancy (**Table 1, 3rd and 6th columns**). Like in the flaming experiments, CCNC derived κ values from most smouldering experiments, which relatively have lower BC contents, shifted also positively from the corresponding chemical-composition based κ values. The magnitude of the shifts did not show any clear burn phase dependence either. The relative positions of the predicted median κ from the CCNC median κ were -0.070 and -0.023 for the flaming experiments; -0.021, +0.008; -0.098; -0.036 for the smouldering experiments. Of the mean κ values, the distance of the predictions from the corresponding CCNC κ values were -0.121 and -0.018 in flaming experiments, while -0.114, -0.040; -0.218; -0.174 in smouldering experiments. On the other hand, just like the predicted κ values across the six different experiment types, the absolute values of mean CCNC-derived κ display pronounced burn-phase-dependent behaviour (discussed in **Sect. 3.4**), even though the externally mixed non-hygroscopic black carbon particles are excluded from the CCNC κ determination. These two observed patterns indicate that burn-phase-dependent characteristics persist in CCNC-derived κ, and simple removal of non-activating black carbon was not proven as a strong positive shift driver in the current study and dataset.

This conclusion is further supported by sensitivity tests in which BC was treated as entirely externally mixed and non-hygroscopic particles (Supplementary Information, Table S11). It can be seen from the table that removing black carbon from the prediction, instead of increasing the accuracy, worsens the accuracy of the prediction relative to the CCNC κ. This was especially for the flaming experiments with high BC content. The burn phase separation pattern of the predicted κ values also flipped after the BC exclusion where the flaming κ values were now higher than the smouldering κ values (Supplementary Information, Fig. S13). This pattern was now in contradiction with the burn phase separated pattern of the CCNC κ values. The suspected cause of these both reversed and higher values of the BC-excluded predicted κ of flaming experiments was the higher inorganic: organic ratio of these experiments compared to the smouldering experiments. Across the flaming experiments, the prediction accuracy errors changed from underpredicting the CCNC κ as much as 23.17% and 4.91% to overpredicting the CCNC κ as much as 164.93% and 233.41% after the BC exclusion, for flaming hardwood and flaming softwood experiments, respectively.

Lastly, SP2 measurements indicate the presence of coated BC particles in some flaming experiments, with coating thickness values exceeding unity, even until more than 1.5. This result suggests that a fraction of BC is internally mixed and may contribute to particle hygroscopicity. However, this complexity is not explicitly represented in the simplified treatment of BC

https://doi.org/10.5194/egusphere-2026-2723
Preprint. Discussion started: 13 July 2026

in composition-based predictions and does not alter the conclusion that BC treatment alone cannot account for the observed inter-method.

3.5.2. Role of Size-Related Factors – Qualitative Check for HTDMA versus prediction

In the present study, HTDMA-derived κ values are number-weighted, whereas AMS–SP2-based κ predictions are inherently mass-weighted. In addition, the effective particle size represented by the HTDMA number-weighted mean depends on the discrete particle sizes selected for measurement. When hygroscopicity is size-dependent, the differences in size representation between the HTDMA and the prediction can, in principle, contribute to discrepancies between measured and predicted κ values. To evaluate the relevance of such size-related effects, two complementary aspects were examined: (i) the representativeness of the HTDMA number-weighted mean particle size relative to the mean size of the complete particle number size distribution measured by the SMPS (Supplementary Information, Fig. S7a), and (ii) the AMS-SP2 mass-weighted composition-based predicted κ values compared to the HTDMA measured discrete size κ values at two different sizes of 75 nm and 110 mm. (Supplementary Information, Fig. S7b). Across most experiment types, the HTDMA-represented mean particle sizes were smaller than the corresponding number-weighted-SMPS-derived mean sizes. This indicates that HTDMA measurements generally emphasize smaller particles, with even larger negative size shifts, compared with those that dominate the bulk mass relevant to AMS–SP2 predictions. Size dependence of the HTDMA κ values was observed mostly in flaming softwood, leaves, and smouldering softwood with lower HTDMA mean κ values at 110 nm than at 75 nm. (Supplementary Information, Fig. S7a and S7b).

Under a framework in which κ decreases with increasing particle size, this mismatch in size representation would be expected to bias number-weighted HTDMA κ values toward higher values relative to mass-weighted predictions, assuming uniform particle density across sizes. Such behaviour is observed only in the flaming-softwood experiments, where HTDMA-derived κ exceeds the predicted κ. In contrast, for many experimental types, measured HTDMA κ values remain systematically lower than predicted values, despite evidence of size-dependent hygroscopicity. This indicates that particle size representation alone cannot explain the observed discrepancies between HTDMA-derived and AMS–SP2-predicted κ values.

Supplementary Information, Fig. S8 (a) and (b), provide insights into how the HTDMA mass-weighted mean sizes in the present dataset differ from the corresponding SMPS mean particle mass size distributions in the leaves experiments, as examples. Based on the Fig. S8 (a) and (b), the differences between the two mean sizes were even larger than those of the corresponding number-weighted approaches. The difference can be as much as a 250 nm negative shift in the HTDMA mass-weighted mean sizes relative to the bulk SMPS mass-weighted mean sizes. As a note, the SMPS mass-distribution-based mean size values were obtained by converting the mean number-size distribution, assuming a constant effective density of 1.3 g/cm3. This constant or uniform value may not have been accurate, especially across different time points or aging stages, and across

https://doi.org/10.5194/egusphere-2026-2723
Preprint. Discussion started: 13 July 2026

different fuels and burning phases. Supplementary Information, Fig. S8 (c) provides the mean HTDMA κ values distribution using the mass-weighted instead of the number-weighted. It can clearly be seen from Fig. S8 that the median κ value of the flaming softwood is now below 0.1, compared to this value in **Fig. 3b**, which is above 0.1.

Overall, the size-resolved analyses demonstrate that size-dependent hygroscopicity and whether to use number- or mass-weighted mean calculations can influence κ comparisons in specific cases; however, they are still insufficient to explain all discrepancies, especially the variability across different burn phases and fuel types.

3.5.3. Role of Size-Related Factors – Quantitative Check for HTDMA versus prediction

Table S12**.** reports the fraction percentage of the lost error from the total initial error of the bulk prediction accuracy in predicting the discrete size HTDMA κ values obtained by changing the particle size from one that has lower HTDMA-prediction agreement to another particle size with better agreement. The two compared particle sizes were 110 nm and 75 nm. This is to illustrate how large the improvement that can be achieved by selecting a more suitable tested particle size of the HTDMA measurement. It is important to remember, however, that the main results of HTDMA κ values to be compared with either CCNC κ or predicted κ values in this current study (**Table 1, Sect. 3**) were number-weighted mean values calculated from across several tested particle sizes, instead of directly using the individual size κ values. Therefore, the results in Table S12 did not provide a direct explanation for the discrepancies in the mean or median κ values investigated in this study. (**Table 1, Sect. 3**).

Based on Table S12, the drops in the prediction error values (%) achieved by selecting the size with closer κ values between 75 nm and 110 nm to the corresponding bulk predicted κ values can be as much as around 15-85% from the total initial error. This indicates that the choice of the dry size in an HTDMA κ measurement can lead to significant differences in the agreement with predicted κ. However, it is important to note that the improvement is still often only marginal. In the case of a peat or a smouldering-hardwood experiment, even choosing the size with better agreement between 110 nm and 75 nm leads to a residual error of several thousand % relative to the predicted value. This is because of the extremely small κ measured under sub-saturated conditions and a correspondingly higher composition-based prediction of κ. The remaining error not covered by the size adjustment indicates the presence of other factors affecting the discrepancy between the measured κ values and the bulk mass weighted predicted κ values, other than the coupling factor between the size dependence of hygroscopicity and the size representation difference issue.

Additionally, in the current study, with the selected number-weighted HTDMA particle sizes, the size dependence of hygroscopicity did not appear to significantly affect the discrepancy between the HTDMA κ values and either the predicted or CCNC κ values. This was illustrated by Fig. S12 (a) and (b) in the Supplementary Information. Figure S12 (a) and (b) provide

https://doi.org/10.5194/egusphere-2026-2723
Preprint. Discussion started: 13 July 2026

the regression linear relationship between the magnitude of the hygroscopicity's size dependence represented through the absolute % difference between the κ values at 110 nm and at 75 nm, with the resulting bulk CCNC κ versus number-weighted HTDMA κ values or bulk predicted κ values versus the HTDMA number-weighted κ values. The R^2 values for these two relationships were small: 0.1247 and $5x10^{-7}$ for HTDMA-CCNC and Predicted-HTDMA, respectively, showing very weak relationships. It could mean that the selected particle sizes were already appropriate and sufficient in many experiments in the current study, and/or that other factors contributed more to the observed inter-method discrepancies. In summary, the choice of size makes very little improvement in the reconciliation of the HTDMA number-weighted mean measured hygroscopicity and bulk mass-weighted predicted hygroscopicity, particularly for small measured hygroscopicity.

Table S13 shows the prediction error that can be achieved by changing the mean calculation approach of the HTDMA κ values from number-weighted to mass-weighted mean calculation. Based on the Table S13, the prediction accuracy generally became worse when changing the calculation approach from number-weighted to mass-weighted. This was despite the aim of trying to more realistically approach the mass-weighting implicit in the AMS-SP2 based prediction. Based on the Table S13, improved accuracy of the prediction relative to the corresponding number-weighted HTDMA mean κ values up to 80% error reduction from the initial total error was only observed in flaming-softwood experiments, either photo-aging or non-photoaging, and in one experiment date of the smouldering-softwood experiments with only about 29.46% error loss from initial total error. It is important to note, however, that the rough mass-weighted calculation of the HTDMA mean κ values in current study used assumption of uniform and constant particle effective density of 1.3 g/cm^3 to convert the SMPS number size distribution to mass size distribution which may not be significantly accurate.

To recap, particle size selection is an important issue when interpreting the discrepancy either between discrete size HTDMA κ or across-sizes- (number or mean)-weighted-mean κ and CCNC mean κ; or between the HTDMA mean κ and predicted mean κ. At a discrete size, selecting incorrect size of the HTDMA κ to be compared with the bulk predicted κ can contribute to up to 85% (maximum observed contribution) of the prediction accuracy error. This high contribution can then also contribute to the discrepancy between the predicted κ and CCNC κ in relatively also a high percentage. Once averaged across sizes, the discrepancy will first depend on how close the size represented by the mean value that was obtained through either number- or mass-weighted in the HTDMA mean κ calculation, with the mean size represented by either the CCNC κ value or prediction κ value determination. However, it is important to note that better or more accurate and comparable size representation does not guarantee better or improved agreement among methods. It just leads to more trusted and reliable discrepancies. The discrepancies themselves could instead become bigger if indeed measurement regime factors exist contributing to the discrepancies. Finally, as previously discussed through the correlation's investigation, in this current study, coupled factors between size dependence of the hygroscopicity and size representation issue was not the most dominant affecting factor of the observed discrepancies.

https://doi.org/10.5194/egusphere-2026-2723
Preprint. Discussion started: 13 July 2026

3.5.4. Size Related Factor's Effect Discussion for CCNC versus Prediction

In contrast to HTDMA, CCNC measurements characterize particle activation in a polydisperse aerosol population under a fixed effective supersaturation (SSeff). Although CCNC-derived κ values are often interpreted as representing bulk aerosol hygroscopicity, the inferred κ is in practice governed primarily by particles near the activation diameter at 50% (D50), rather than by the entire size distribution. In this sense, CCNC-derived κ retains an implicit number-weighted character, determined by activation probability rather than explicit size selection. By comparison, κ values derived from AMS–SP2 data are inherently mass-weighted, reflecting chemical contributions dominated by particles near the mass-weighted mean diameter. Although both CCNC and AMS–SP2 approaches are frequently described as providing bulk κ values, they do not represent the same effective particle sizes. Differences between CCNC-derived and predicted κ values, therefore, arise naturally when hygroscopicity is size-dependent or when the aerosol population is not internally mixed.

Under such conditions, D50-related effects influence CCNC–AMS κ discrepancies through two complementary mechanisms. First is related to the number-weighted activation criterion versus the mass-weighted chemical signal, as mentioned earlier. Secondly, the CCNC–AMS discrepancy is also sensitive to the direction of size-dependent hygroscopicity. In either cases of decreasing or especially increasing hygroscopicity with particle size increase, the resulting activation curve behaviour can mimic the curve of an internally mixed aerosol population, even though it is actually driven by size-dependent effects, leading to shifted/biased κ values. Externally mixed aerosol populations, i.e. more than one range of hygroscopicity values for one same particle size, can further complicate this interpretation. In the present study, neither size-resolved CCNC activation measurements nor size-resolved chemical composition data were available. A more detailed, case-by-case discussion of these mechanisms is provided in the Supplementary Information, Notes S5, including the data processing approach used in this current study while handling SPAR curves with apparent two spikes.

3.5.5. Role of the used κ_{org} and plausible variation of the κ_{org} value- General investigation

Based on **Fig. 3** in **Sect. 3.1**, HTDMA median κ values in all experiments are lower than the chemical composition-based predicted κ values, except those of flaming-softwood experiments. This was despite the presence of size-related factor(s) suspected as factor(s) leading to higher measured number-weighted HTDMA κ values than their real bulk values, as discussed in previous subsection. Kim N et al (2017) in their study suspected that overestimated κ values in prediction calculations, compared to HTDMA dataset values, could be likely caused by overly high κ_{org} used in the formula. A similar issue might explain the current study's findings in most experiments except the flaming-softwood experiments (though reduction in κ_{org} would lead to increased underprediction of the κ values relative to the CCNC κ values). Varying discrepancies between measured and predicted HTDMA κ values across different experiment types, including the exceptional pattern of the flaming-

https://doi.org/10.5194/egusphere-2026-2723
Preprint. Discussion started: 13 July 2026

softwood experiment, indicate that κ_{org} values may differ depending on the fuel type or burning conditions, though plausible variation in κ_{org} applied in the current study is unable to bring better agreement between the HTDMA κ and prediction κ.

In this study, efforts to use linear regression to determine fractional κ values for each experiment type were inconclusive, likely due to insufficient dynamic range (see Table S7-S8 and Fig. S9). Therefore, an effort to minimize the effect of inappropriateness in applying the selected constant fractional κ values were investigated by widening the predicted hygroscopicity values by varying the fractional κ values across a plausible range for comparison with HTDMA or CCNC measurements. A validation check of the varied κ_{org} presence can also then be done by using a range of available linear regression equations of κ_{org} versus O:C ratio relationships in previous studies. This was done in this current study as a complementary investigation, as provided in Fig. S10(b).

The O:C used in the current validation check is not the directly measured value, but rather the f44 versus O:C functional relationship given by the equation of Aiken, A. C., et al (2008): $f(x)=(0.0382\pm0.0005)x+(0.0794\pm0.0070)$ where f(x) is the O:C ratio and x is the f44 (m/z 44 mass divided by OA mass). Meanwhile, the equation used to convert the O:C ratio was $\kappa_{org} = 0.18\times O/C + 0.03$, according to $\kappa_{org} = (0.18\pm0.04)\times O/C + 0.03$ by Lambe, A. al. (2011) that was generated over measured O/C ratios ranging from 0.05 to 1.42. This coefficient value of 0.18 was roughly similar to the finding of Thalman et al. (2017), which reported a consistent value of κ_{org} ~0.15 that corresponded to O:C ratio ~0.8 (κ_{org} =0.1875 x O/C). On the other hand, a higher coefficient like in the equation of Chang, et al., (2010): $\kappa_{org}=(0.29\pm0.05)\cdot(O/C)$ for the O:C ratio ranging from 0.3 to 0.6, was not used in the current study, due to its narrower O:C ratio values range used in that equation's generation, compared to the O:C ratio range in the current study's dataset. That coefficient value of 0.29 was actually similar to the recently published value that constructed an equation for final κ (instead of κ_{org}) versus O:C ratio: $\kappa = 0.31 \pm 0.02\ (O/C) - 0.05 \pm 0.02$ of biomass burning particle (Bai, B., et al, 2026). Additional calculations using that equation could maybe be conducted in the present dataset to obtain the final κ values compared to those from three methods of the current study focus. However, it is important to note that many other published articles have found that the hygroscopicity of the organic fraction (*thus likely also the overall hygroscopicity, especially of particles with complex change of chemical mass fraction composition, such as inorganic: organic and/or organic: BC ratio*) is not solely determined by oxidation state as reflected by O:C ratio values (Han, S., et al 2021), so that these kind of equations were recommended to be used as an approximate guidance only. (Chang, R. Y.-W., et al 2010).

Based on the Fig. S10(b). , the observed burning phase-separated patterns show that flaming experiments have higher κ_{org} values than smouldering experiments, regardless of fuel type, with peat having the lowest κ_{org}. These κ_{org} patterns were not like either CCNC κ or AMS-SP2 κ burn phase-separated patterns that have a reverse burn phase separation pattern, i.e., higher smouldering κ than flaming κ. Additionally, based on the ZSR equation, constant or similar values of other components – inorganic hygroscopicity and mass fractions of either organic or inorganic- like within the same burn phase, should drive the resulting κ values' pattern to follow the κ_{org} values' pattern. However, the CCNC κ in this study did not follow the pattern of

https://doi.org/10.5194/egusphere-2026-2723
Preprint. Discussion started: 13 July 2026

the calculated κ_{org} values, assuming those values were roughly accurate, at least in their inter-experiment-type patterns. For example, the highest smouldering κ among the CCNC smouldering κ values was not from smouldering-softwood as expected. Compared to HTDMA-derived κ, the patterns (Fig. S10(b)) seemed roughly similar to the κ_{org} values, except for the flaming hardwood experiment. These results may suggest the presence of other fuel- and burn-phase-dependent, non-systematic factors contributing to variability, particularly in the measured CCNC κ values, in addition to the variability in the particles' κ_{org} values not captured by bulk chemical composition alone. Droplet activation in this current study may also be controlled by population heterogeneity and/or activation-related processes specific to supersaturated conditions.

3.5.6. Quantitative Check of the influence of O:C ratio Informed Organic κ Adjustment

Based on the bulk averaged O:C ratio AMS f44-based calculated values in Fig. S10 (a) and the corresponding equation based derived κ_{org} values in Fig. S10 (b), new predicted κ values were calculated as in the Table S14. Based on Table S14, the use of the new κ_{org} values as mentioned above, instead of the single κ_{org} value = 0.1, improved the accuracy of the prediction relative to the corresponding HTDMA κ in only some experiments. The improvement could achieve a reduction of up to 46.95% (at the highest) from the initial total error. Consistent direction of the accuracy change, which was a positive direction or improvement, was observed in only the prediction of HTDMA κ of peat experiments across all repetitions and aging time points. Compared to the CCNC κ values, chemical composition-based κ predictions using the new κ_{org} values showed better agreement in only a few experiments too. However, the contribution percentages of the error loss relative to the initial total error (%) in predicted versus CCNC measurement comparisons were much lower, achieving mostly less than 5% loss of prediction accuracy, with only two experiment showing an error reduction of 9.23% and 22.99%.

The lower sensitivity of the CCNC κ values could be caused by their significantly higher discrepancies to the predicted κ values compared to the corresponding discrepancies of HTDMA κ values to the predicted κ values. For example, in a flaming-softwood experiment on 07 April 2022, the gaps between HTDMA κ and the predicted κ changed from +0.032 to +0.025 (absolute delta of the deviation = 0.007), equal to a reduction of the prediction accuracy error as much as 15.91% from the total initial error. Meanwhile, the gaps between CCNC κ and the predicted κ changed from +0.077 to +0.070 (absolute delta of the deviation = 0.007), equal to a reduction of the prediction accuracy error as much as 1.63% from the total initial error. Similarly, in a leave experiment on 29 September 2022, a change in the deviation of the CCNC κ relative to the predicted CCNC κ from +0.081 to +0.119 corresponded to just 0.147% reduction in error, but the same shift (-0.069 to -0.031) corresponded to a 9.82% error loss of the prediction accuracy relative to the HTDMA κ.

3.5.7. Other Factors: What remained and not tested Factors - Regime Dependent Hygroscopicity

https://doi.org/10.5194/egusphere-2026-2723
Preprint. Discussion started: 13 July 2026

This current subsection discusses the not currently tested factors which are measurement regime dependent factors. As mentioned in earlier discussion, the present data sets showed roughly consistent direction of discrepancies at which CCNC κ values were always higher than HTDMA κ values. This kind of discrepancy pattern was also observed in several studies of especially organic-rich or complex mixture, indicating measurement-regime-dependent-behavior (Wu, Z., et al 2013; Pajunoja, A., et al 2015; and Jurányi, et al 2009)

The HTDMA-derived κ represents equilibrium water uptake at ~90% RH, whereas in biomass burning aerosols dominated by organic material, hygroscopic growth under subsaturated conditions can be suppressed by thermodynamic constraint, such as limited solubility leaving the particles into partially dissolved condition, and kinetic limitation, such as diffusion-limited water uptake driven by certain particle phase states. The water uptake restricting particle phases could be in form of amorphous semi-solid or solid (i.e., glassy or crystalline state) (Koop, T., et al, 2011). Depending on the microstructure and viscosity, Mikhailov, E. et al (2009) further classified amorphous phases into: gels or viscous liquids, rubbers, and glasses/ultra-viscous amorphous state. The restricted water uptake conditions caused by the particle phase state then led to lower apparent κ values. On the other hand, CCNC-derived κ reflects activation behaviour near or above supersaturation. During CCN activation, the Köhler framework amplifies both solute (Raoult) and surface tension (Kelvin) effects, particularly near the critical point, while these two effects can be suppressed or even totally disappeared at ~90% RH where particles exist in a more concentrated conditions with potential presence of incomplete dissolution and phase limitations.

Another factor, which is instrumental and kinetic related effect – specifically, organic co-condensation effect, could also exist, contributing to the inter-method discrepancies, though not tested here. In cases where CCNC κ becomes higher than HTDMA κ because of surface tension presence and absence in CCNC measurement and HTDMA measurement, respectively, it seems reasonable to expect that the co-condensation that can potentially happen in HTDMA measurement only will reduce the HTDMA-CCNC discrepancies. More detailed explanation of each of the factors mentioned in this subsection are in Supplementary Information, Note S7.3

3.5.8. Limitations of composition-based κ prediction

This subsection discusses limitations of composition-based κ prediction in capturing factors that affect the HTDMA and/or CCNC κ as detailed in previous subsections. In addition to measurement regime effects, discrepancies between predicted and measured κ values reflect limitations in the composition-based framework. The prediction relies on simplified assumptions, including fixed κ values for each component, an ideal internal mixing rule, and the neglect of surface tension and phase-state effects, as well as potential neglect of gas-particle partitioning of semivolatile organic vapors (Wu et al., 2013). Additionally, the current study uses mass fraction approaches instead of volume fractions, assuming comparable or similar densities across components (Gunthe et al., 2009), which is a reasonable approximation for particles consisting mostly of organics. Besides,

https://doi.org/10.5194/egusphere-2026-2723
Preprint. Discussion started: 13 July 2026

among particles with similar component densities, systematic bias can arise when converting masses to volumes, due to factors such as composition-dependent instrument collection efficiencies (Brock et al., 2011).

The use of a constant κ value for organic aerosol ($\kappa_{org} \approx 0.1$) does not capture the variability of biomass burning organics, which depend strongly on fuel type and combustion conditions (Bougiatioti et al., 2016; Saleh et al., 2013). Meanwhile, enhanced CCN activity driven by surface-tension reduction is not accounted for (Xiong et al., 2022), contributing to the underestimation of κCCNC. The assumption of ideal mixing further limits predictive accuracy, as systematic bias can result. Interactions between inorganic salts, organic compounds, and black carbon can produce non-linear hygroscopic behavior, challenging the ideal internal mixing assumption due to factors such as core-shell morphology and the kinetic limitations (Wang et al., 2021), dry organic-inorganic particles non-ideal mixing with density deviations of up to 20% (Vokes et al., 2022), phase separation, partial solubility, and surfactant partitioning phenomenon. Further, potential external mixing contributing to the bulk chemical composition measurements was not accommodated in the ZSR-based internal mixing rules. Lastly, the prediction does not account for particle phase state or kinetic limitations. Semi-solid or viscous particles may not fully equilibrate with water vapor at subsaturated conditions, reducing observed growth relative to predicted values.

Assuming that the varied process mentioned above occurs only among the organic components, not including intercomponent interactions, those processes should only affect and be sufficiently accommodated in the κ_{org} parameter. In the current study, replacing the uniform κ_{org} value with the O:C ratio-based κ_{org} still couldn't sufficiently and consistently capture the fuel-and-burn-phase dependent discrepancies caused by the factors in the previous paragraph, either when compared to HTDMA or CCNC, at which the prediction-measurement discrepancies were not only varied in terms of magnitudes, but also in directions, i.e., lower or higher, relative to the prediction.

Finally, differences in the size representation—bulk mass-based composition of the prediction versus either sizes selected using a number-weighted approach in the HTDMA or a size-number distribution-based approach in the CCNC measurements—may introduce further discrepancies when hygroscopicity varies across the particle population. Overall, composition-based κ should be interpreted as a first-order estimate. The observed deviations highlight the importance of processes not captured by simplified mixing frameworks. **Table 5** below provides a summary of factors with different and/or contradicting effects on the different measurement instruments or on the prediction.

Table 5. Summary of contradicting effects of some factors on the HTDMA measured κ values and CCNC measured κ values

Factors and Validity in this Current Study	**The contradicting effect**
Presence of an external mixture – Slightly validated	$\kappa_{AMS\text{-}SP2}$ is more similar to $\kappa_{HTDMA,}$ which uses piecewise linear fitting to accommodate all the substances with

https://doi.org/10.5194/egusphere-2026-2723
Preprint. Discussion started: 13 July 2026

	different hygroscopicity, than to κ_{CCN}, which ignores the non-hygroscopic fraction
Presence of surface-active substances – Assumed or Not Validated	Potentially lower or keeping constant the κ_{HTDMA}, yet increasing the κ_{CCNC}, not affecting the $\kappa_{AMS\text{-}SP2}$
Presence of condensable organic gases – Assumed or Not Validated	Not affect κ_{CCNC}, nor $\kappa_{AMS\text{-}SP2}$, but can improve the κ_{HTDMA}
Particles' phase state and morphology – Assumed or Not Validated	Likely influence κ_{HTDMA} significantly, but not the κ_{CCNC}. For example, the solid phase of the particles in the HTDMA measurements may limit the particles' ability to take up water vapor further, yet in the CCNC measurement, this barrier was overcome through fast water droplet activation; not affect $\kappa_{AMS\text{-}SP2}$.

3.5.9 Direction for Future Work

Although this study has identified several potential drivers of the discrepancies among κ values derived from CCNC, HTDMA, and composition-based prediction, further work is required to quantify these effects more systematically and rigorously, particularly for processes that were not explicitly isolated here. A more systematic experimental framework is proposed, consisting of four complementary sets of experiments for each fuel and burn condition to first minimize discrepancies associated with particle size representation and mixing state, then investigate and isolate discrepancies caused potentially by organic-and water vapor co-condensation differences in the HTDMA and CCNC instruments. (Supplementary Information, Notes S8)

Once the issue of the two instrumental systems' difference regarding the organic-and-water vapor co-condensation possibility or presence is isolated or diminished, whereas discrepancies associated with particle size representation and mixing state are minimized, it may become possible to derive a quantitative correction framework linking κ values obtained from different measurement approaches. Such a framework, developed within a unified experimental system, could enable conversion between HTDMA-, CCNC-, and composition-derived κ values. This would allow more consistent application of hygroscopicity data, for example, using HTDMA-derived κ for subsaturated processes such as visibility and CCNC-derived κ for cloud activation and aerosol–cloud interaction studies.

Lastly, ranges of measurements (Supplementary Information, Notes S8) not conducted in the current study were suggested to further explore the discrepancy factors more thoroughly and deeply. Additionally, particle density measurements should probably be useful if HTDMA mass-weighted averaged values are also calculated and compared in addition to the HTDMA

https://doi.org/10.5194/egusphere-2026-2723
Preprint. Discussion started: 13 July 2026

number-weighted averaged, to avoid any bias caused by the assumption of uniform effective particle density in the SMPS number concentration to SMPS mass concentration conversion.

Conclusion

This study investigated the hygroscopicity (κ) of submicron biomass-burning aerosols generated from peat, leaves, hardwood, and softwood under flaming and smouldering conditions using three approaches: HTDMA measurements, CCNC measurements, and AMS–SP2 composition-based prediction. All experiments were conducted within a consistent experimental framework, allowing direct comparison of both κ values and the underlying mechanisms controlling them. In general, CCNC-derived κ exceeds HTDMA-derived κ, with composition-based predictions falling in between. These discrepancies reflect the fundamentally different aerosol properties emphasized by each method. Composition-based κ values are primarily governed by burn-phase-dependent bulk chemical composition, whereas CCNC-derived κ reflects activation behaviour under supersaturation and HTDMA-derived κ reflects subsaturated hygroscopic growth. Both the magnitude and direction of discrepancies vary across fuel types and combustion conditions. Clear burn phase separation, at which smouldering particles generated higher κ values, was observed in both the CCNCC measurement and the chemical composition-based retrieval.

The relative ordering of fuels differs between methods. Under supersaturated conditions, smouldering aerosols, particularly from peat and leaves, exhibit the highest κ values, whereas flaming aerosols show lower values. Under subsaturated conditions, κ shows greater fuel dependence, with peat exhibiting the lowest values, consistent with its low effective organic hygroscopicity and the likely presence of a semi-solid particle phase. This contrasting behaviour, particularly for peat, highlights the role of regime-dependent processes affecting aerosol water uptake. The mean values of each method under flaming and smouldering burn phases in sequence were 0.040-0.068 and 0.049-0.123 for HTDMA; 0.105-0.161 and 0.163-0.238 for CCNC; then 0.060-0.068 and 0.114-0.133 for AMS-SP2 chemical composition-based predictions, respectively.

Several suspected factors contributing to the discrepancies among measurements were investigated. The coupling effect between size representation and κ size dependence was quantitatively observed as affecting the HTDMA-CCNC κ discrepancies. However, the influence was small compared to the total observed discrepancies. Similarly, the contributing effect of the presence of externally mixed non-hygroscopic BC particles to the discrepancies seemed not significant. The possible cause of the insignificant contribution of the BC content presence to the HTDMA-CCNC discrepancy was the likely presence of a significant fraction of the BC content in the form of coated BC particles, which likely reduces its impact on any difference in κ values caused by the CCNC data processing nature that excludes the non-hygroscopic fraction from the κ difference.

https://doi.org/10.5194/egusphere-2026-2723
Preprint. Discussion started: 13 July 2026

Among the tested measurement versus prediction factors, κorg seemed to be a more important factor than the size-related factor. However, not all fuel types and burn phases produced particles with strong O:C ratio versus κorg correlations. Peat became the only experiment type consistently benefited, with a 16–59% improvement, while substantial residual discrepancies remained, from using an O:C ratio-informed κorg instead of a constant κorg of 0.1. Additionally, changing the initially used uniform κorg of 0.1 to more experiment-type dependent values in the prediction affects the HTDMA versus prediction discrepancies noticeably, but affects only slightly the CCNC versus prediction discrepancies. The coupling between size representation and intrinsic size dependence of hygroscopicity may also contribute to the discrepancies, particularly when particle sizes are not sufficiently and appropriately selected, tested, and accounted for in HTDMA-derived mean κ values. However, this effect does not appear to be the most significant driver in the present dataset. Lastly, the quantitative investigation in this study confirmed the importance of the BC fraction inclusion in the AMS-SP2-based κ prediction of the BB particles.

Overall, the results demonstrate that hygroscopicity in biomass-burning aerosols is a regime-dependent property rather than a single intrinsic parameter. Although not explicitly isolated or investigated in the current study, the observed significant divergence between subsaturated and supersaturated κ values suggests additional discrepancies affecting factors related to different physicochemical processes that dominate across regimes. The factors include those related to a kinetic limitation on water uptake (e.g., particle phase state) and those related to activation-related processes, including both surface tension reduction and bulk–surface partitioning. Taken together, these findings highlight that κ cannot be treated as a method-independent quantity for biomass-burning aerosols. Instead, regime-aware parameterizations are required, explicitly accounting for size–composition coupling, mixing state, and the physicochemical processes governing both subsaturated water uptake and cloud droplet activation.

Appendix A

All the additional materials, such as explanations, figures, and tables, are provided in a separate file available in the link as mentioned in “Supplement Link” section.

Code and data availability

The code and data are available at Zenodo: https://doi.org/10.5281/zenodo.20695234.

Supplement link

The link to the supplement will be included by Copernicus.

Author contributions

https://doi.org/10.5194/egusphere-2026-2723
Preprint. Discussion started: 13 July 2026

SAS and **GM** conceived the study. **SAS** conducted the HTDMA, CCNC, and AMS data processing, analysis, and interpretation, then wrote the whole manuscript with feedback from all co-authors. **HW** provided the SP2 ready-to-use processed data. **DH and YW** provided insight on CCNC and HTDMA data processing. **DH** helped with some issues with the IGOR toolkit use of the HTDMA or CCNC data processings. **GM, JA, AV, DH,** and **HW** provided insights on the whole data analysis and interpretation. **SAS, AV, OEO,** and **HW** did the daily BB experiments, **YS** participated in the September daily BB experiments, **SHB** gave some proofreading/editorial comments, and **HC** participated in giving later-stage supervision to the first author in this manuscript finalisation, as well as coordination with the other co-author(s). **PJG** participated, initiated, coordinated, and led the earlier meetings and the written discussions of the UoM April 2022 BB campaign preparation. **MF** assisted with any technical issues with instruments, such as the CCNC system.

Competing interests

At least one of the (co-)authors is a member of the editorial board of ACP.

Disclaimer

Copernicus Publications adds a standard disclaimer: "Copernicus Publications remains neutral with regard to jurisdictional claims made in the text, published maps, institutional affiliations, or any other geographical representation in this paper. While Copernicus Publications makes every effort to include appropriate place names, the final responsibility lies with the authors. Views expressed in the text are those of the authors and do not necessarily reflect the views of the publisher."

Financial support

The Manchester Aerosol Chamber receives funding from the Horizon 2020 Research and Innovation Framework Programme, H2020-INFRAIA-2020-1, Sustainable Access to Atmospheric Research Facilities (ATMO-ACCESS) (grant agreement no. 101008004). **Sara Aisyah Syafira** acknowledges studentship support from the Indonesia Endowment Fund for Education (Lembaga Pengelola Dana Pendidikan, LPDP) with sponsorship reference number LOG-1962/LPDP.3/2023, and **Osayomwanbor Oghama** acknowledges studentship support from the Tertiary Education Trust Fund (TETFund), Nigeria, with sponsorship reference number TETF/ES/UNIV/DELTA STATE/TSAS/2019. **Aristeidis Voliotis** acknowledges funding support from the Natural Environment Research Council (NERC) through the UK National Centre for Atmospheric Science (NCAS).

https://doi.org/10.5194/egusphere-2026-2723
Preprint. Discussion started: 13 July 2026

References

Alfarra, M. R., Coe, H., Allan, J. D., Bower, K. N., Boudries, H., Canagaratna, M. R., Jimenez, J. L., Jayne, J. T., Garforth, A. A., Li, S.-M., & Worsnop, D. R.: Characterization of urban and rural organic particulate in the Lower Fraser Valley using two Aerodyne aerosol mass spectrometers,
Atmospheric Environment, 38(34), 5745–5758. https://doi.org/10.1016/j.atmosenv.2004.01.054, 2004.

Allan, J. D., Delia, A. E., Coe, H., Bower, K. N., Alfarra, M. R., Jimenez, J. L., Middlebrook, A. M., Drewnick, F., Onasch, T. B., Canagaratna, M. R., Jayne, J. T., and Wornsop, D. R.: A generalised method for the extraction of chemically resolved mass spectra from aerodyne aerosol mass spectrometer data – Technical note, Journal of Aerosol Science, 35, 909-922, doi:10.1016/j.jaerosci.2004.02.007, 2004.

Andreae, M. O.: Emission of trace gases and aerosols from biomass burning – an updated assessment, Atmos. Chem. Phys., 19, 8523–8546, https://doi.org/10.5194/acp-19-8523-2019, 2019.

Bai, B., Singh, A., Xu, T., Stamatis, C., Lu, K., Shin, N., Glenn, C. K., Hajj, O. E., Kumar, R. V., Anosike, A., Abdurrahman, M. I., Gunthe, S. S., O'Brien, J. H., Isaacman-VanWertz, G., Saleh, R., Ng, N. L., & Liu, P.: Hygroscopicity and Cloud Condensation Nuclei Activity of Fresh and Aged Biomass Burning Particles, ACS ES&T Air, 3, 697–709, https://doi.org/10.1021/acsestair.5c0017, 2026.

Bougiatioti, A., Bezantakos, S., Stavroulas, I., Kalivitis, N., Kokkalis, P., Biskos, G., Mihalopoulos, N., Papayannis, A., and Nenes, A.: Biomass-burning impact on CCN number, hygroscopicity and cloud formation during summertime in the eastern Mediterranean, Atmospheric chemistry and physics, 16, 7389–7409, https://doi.org/10.5194/acp-16-7389-2016, 2016.

Brock, C. A., Cozic, J., Bahreini, R., Froyd, K. D., Middlebrook, A. M., McComiskey, A., Brioude, J., Cooper, O. R., Stohl, A., Aikin, K. C., Gouw, J. A. de, Fahey, D. W., Ferrare, R. A., Gao, R. S., Gore, W. J., Holloway, J. S., Hübler, G., Jefferson, A., Lack, D. A., Lance, S., Moore, R. H., Murphy, D. M., Nenes, A., Novelli, P. C., Nowak, J. B., Ogren, J. A., Peischl, J., Pierce, R. B., Pilewskie, P., Quinn, P. K., Ryerson, T. B., Schmidt, K. S., Schwarz, J. P., Sodemann, H., Spackman, J. R., Stark, H., Thomson, D. S., Thornberry, T., Veres, P. R., Watts, L. A., Warneke, C., and Wollny, A. G.: Characteristics, sources, and transport of aerosols measured in spring 2008 during the aerosol, radiation, and cloud processes affecting Arctic Climate (ARCPAC) Project, Atmospheric chemistry and physics, 11, 2423–2453, https://doi.org/10.5194/acp-11-2423-2011, 2011.

Cai, M., Tan, H., Chan, C. K., Qin, Y., Xu, H., Li, F., Schurman, M. I., Liu, L., & Zhao, J.: The size-resolved cloud condensation nuclei (CCN) activity and its prediction based on aerosol hygroscopicity and composition in the Pearl Delta River (PRD) region during wintertime 2014, Atmos. Chem. Phys., 18, 16419–16437, https://doi.org/10.5194/acp-18-16419-2018, 2018.

https://doi.org/10.5194/egusphere-2026-2723
Preprint. Discussion started: 13 July 2026

Carrico, C. M., Petters, M. D., Kreidenweis, S. M., Sullivan, A. P., McMeeking, G. R., Levin, E. J. T., Engling, G., Malm, W. C., & Collett, J. L.: Hygroscopic growth and cloud condensation nuclei activity of biomass burning aerosol, Atmospheric Chemistry and Physics, 10, 5165–5177, https://doi.org/10.5194/acp-10-5165-2010, 2010.

Chang, R. Y.-W., Slowik, J. G., Shantz, N. C., Vlasenko, A., Liggio, J., Sjostedt, S. J., Leaitch, W. R., and Abbatt, J. P. D.: The hygroscopicity parameter (κ) of ambient organic aerosol at a field site subject to biogenic and anthropogenic influences: relationship to degree of aerosol oxidation, Atmos. Chem. Phys., 10, 5047–5064, https://doi.org/10.5194/acp-10-5047-2010, 2010.

Che, H.C., Zhang, X.Y., Zhang, L. et al. Prediction of size-resolved number concentration of cloud condensation nuclei and long-term measurements of their activation characteristics. Sci Rep **7**, 5819, https://doi.org/10.1038/s41598-017-05998-3, 2017.

Chen, J., Jakob, F. M. O., Voliotis, A., Wu, H., Syafira, S. A., Oghama, O., Shardt, N., Faure, N., Kong, X., McFiggans, G., and Kanji, Z. A.: Ice nucleation abilities and chemical characteristics of laboratory-generated and aged biomass burning aerosols, Environmental Science and Technology, 59, 2575-2586, https://doi.org/10.1021/acs.est.4c04941, 2025.

Chen, J., Budisulistiorini, S. H., Itoh, M., & Kuwata, M.: Roles of relative humidity and particle size on chemical aging of tropical peatland burning particles: Potential influence of phase state and implications for hygroscopic property, Journal of Geophysical Research: Atmospheres, 127, e2022JD036871, https://doi.org/10.1029/2022JD036871, 2022.

Deng, Z. Z., Zhao, C. S., Ma, N., Ran, L., Zhou, G.Q., Lu, D.R., Zhou, X. J.: An examination of parameterizations for the CCN number concentration based on in situ measurements of aerosol activation properties in the North China Plain, Atmos. Chem. Phys., 13: 6227-6237, https://doi.org/10.5194/acp-13-6227-2013, 2013.

Duplissy, J., DeCarlo, P. F., Dommen, J., Alfarra, M. R., Metzger, A., Barmpadimos, I., Prevot, A. S. H., Weingartner, E., Tritscher, T., Gysel, M., Aiken, A. C., Jimenez, J. L., Canagaratna, M. R., Worsnop, D. R., Collins, D. R., Tomlinson, J., and Baltensperger, U.: Relating hygroscopicity and composition of organic aerosol particulate matter, Atmospheric Chemistry and Physics, 11(3), 1155–1165. https://doi.org/10.5194/acp-11-1155-2011, 2011.

Dusek, U., Frank, G. P., Hildebrandt, L., Curtius, J., Schneider, J., Walter, S., Chand, D., Drewnick, F., Hings, S., Jung, D., Borrmann, S., and Andreae, M. O.: Size matters more than chemistry for cloud-nucleating ability of aerosol particles. Science, 312(5778), 1375-1378. https://doi.org/10.1126/science.1125261, 2006.

Engelhart, G. J., Hennigan, C. J., Miracolo, M. A., Robinson, A. L., & Pandis, S. N.: Cloud condensation nuclei activity of fresh primary and aged biomass burning aerosol, Atmospheric Chemistry and Physics, 12(13), 7285–7293, https://doi.org/10.5194/acp-12-7285-2012, 2012.

Evans, R. L., Bryant, D. J., Voliotis, A., Hu, D., Wu, H., Syafira, S. A., Oghama, O. E., McFiggans, G., Hamilton, J. F., and Rickard, A. R.: A semi-quantitative approach to nontarget compositional analysis of complex samples, Analytical Chemistry, 96(46), 18349-18358, https://doi.org/10.1021/acs.analchem.4c00819, 2024.

Evans, R. L., Bryant, D. J., Voliotis, A., Hu, D., Wu, H., Syafira, S. A., Oghama, O. E., McFiggans, G., Hamilton, J. F., and Rickard, A. R.: The importance of burning conditions on the composition of domestic biomass-burning organic aerosol

https://doi.org/10.5194/egusphere-2026-2723
Preprint. Discussion started: 13 July 2026

and the impact of atmospheric ageing, Atmos. Chem. Phys., 25, 4367–4389, https://doi.org/10.5194/acp-25-4367-2025, 2025.

Fan X, Liu J, Zhang F, Chen L, Collins D, Xu W, Jin X, Ren J, Wang Y, Hu H, Li S, Sun Y, Li Z.: Contrasting size-resolved hygroscopicity of fine particles derived by HTDMA and HR-ToF-AMS measurements between summer and winter in Beijing: the impacts of aerosol aging and local emissions, Atmos Chem Phys, https://doi.org/10.5194/acp-20-915-2020, 20, 915–929, 2020.

Ferdousi-Rokib, N., Dutcher, D. D., Malek, K. A., Gohil, K., Raymond, T. M., Pitta, K. R., Freedman, M. A., and Asa-Awuku, A. A.: Salting out and nitrogen effects on cloud nucleating ability of amino acid aerosol mixtures, Environmental Science: Atmospheres, 5, 485-501, DOI: 10.1039/d4ea00128a, 2025.

Gao, R. S., Schwarz, J. P., Kelly, K. K., Fahey, D. W., Watts, L. A., Thompson, T. L., Spackman, J. R., Slowik, J. G., Cross, E. S., Han, J.-H. H., Davidovits, P., Onasch, T. B., and Worsnop, D. R.: A Novel Method for Estimating Light Scattering Properties of Soot Aerosols Using a Modified Single Particle Soot Photometer, Aerosol Sci. Technol., 41, 125–135, doi:10.1080/02786820601118398, 2007.

Garg, P., Wang, S., Oakes, J. M., Bellini, C., and Gollner, M. J.: Variations in gaseous and particulate emissions from flaming and smouldering combustion of Douglas fir and lodgepole pine under different fuel moisture conditions, Combustion and Flame, 263, 1-13. https://doi.org/10.1016/j.combustflame.2024.113386, 2024.

Good, N., Coe, H., and McFiggans, G.: Instrumentational operation and analytical methodology for the reconciliation of aerosol water uptake under sub- and supersaturated conditions, Atmos. Meas. Tech., 3, 1241–1254, https://doi.org/10.5194/amt-3-1241- 2010, 2010a.

Gunthe, S. S., King, S. M., Rose, D., Chen, Q., Roldin, P., Farmer, D. K., Jimenez, J. L., Artaxo, P., Andreae, M. O., Martin, S. T., and Pöschl, U.: Cloud condensation nuclei in pristine tropical rainforest air of Amazonia: size-resolved measurements and modeling of atmospheric aerosol composition and CCN activity, Atmos. Chem. Phys, 9, 7551–7575, https://doi.org/10.5194/acp-9-7551-2009, 2009.

Gunthe, S. S., Rose, D., Su, H., Garland, R. M., Achtert, P., Nowak, AMEa., Wiedensohler, A., Andreae, M. O., & Pöschl, U.: Cloud condensation nuclei (CCN) from fresh and aged air pollution in the megacity region of Beijing, Atmospheric Chemistry and Physics, 9(21), 11053-11073, https://doi.org/10.5194/acp-9-11053-2009., 2009.

Gysel, M., Weingartner, E., & Baltensperger, U.: Hygroscopicity of aerosol particles at low temperatures. 1. New low-temperature H-TDMA instrument: Setup and first applications, Environmental Science & Technology, 36(1), 55-62, https://doi.org/10.1021/es010054o., 2002.

Gysel, M., Crosier, J., Topping, D. O., Whitehead, J. D., Bower, K. N., Cubison, M. J., Williams, P. I., Flynn, M. J., McFiggans, G. B., & Coe, H.: Closure study between chemical composition and hygroscopic growth of aerosol particles during TORCH2, Atmospheric Chemistry and Physics, 7, 6131–6144, 2007.

https://doi.org/10.5194/egusphere-2026-2723
Preprint. Discussion started: 13 July 2026

Gysel, M., McFiggans, G. B., and Coe, H.: Inversion of tandem differential mobility analyser (TDMA) measurements, Journal of Aerosol Science, 40(2), 134–151, https://doi.org/10.1016/j.jaerosci.2008.07.013, 2009.

Han, S., Hong, J., Luo, Q., Xu, H., Tan, H., Wang, Q., Tao, J., Zhou, Y., Peng, L., He, Y., Shi, J., Ma, N., Cheng, Y., and Su, H.: Hygroscopicity of organic compounds as a function of organic functionality, water solubility, molecular weight, and oxidation level, Atmos. Chem. Phys., 22, 3985–4004, https://doi.org/10.5194/acp-22-3985-2022, 2022.

Hass-Mitchell, T., Joo, T., Rogers, M., Nault, B. A., Soong, C., Tran, M., Seo, M., Machesky, J. E., Canagaratna, M., Roscioli, J., Claflin, M. S., Lerner, B. M., Blomdahl, D. C., Misztal, P. K., Ng, Nga. L., Dillner, A. M., Bahreini, R., Russel, A., Krechmer, E., Lambe, A., and Gentner, D. R.: Increasing Contributions of Temperature-Dependent Oxygenated Organic Aerosol to Summertime Particulate Matter in New York City, ACS EST Air, 1, 113-128, https://doi.org/10.1021/acsestair.3c00037, 2024.

He, C.: Radiative properties of atmospheric black carbon (soot) particles with complex structures. In A. Kokhanovsky (Ed.), Springer Series in Light Scattering (pp. 219-255), Cham: Springer. https://doi.org/10.1007/978-3-030-20587-4_5, 2019.

Healy, R. M., Evans, G. J., Murphy, M., Jurányi, Z., Tritscher, T., Laborde, M., Weingartner, E., Gysel, M., Poulain, L., Kamili, K. A., Wiedensohler, A., O'Connor, I. P., McGillicuddy, E., Sodeau, J. R., Wenger, J. C.: Predicting hygroscopic growth using single particle chemical composition estimates, J. Geophys. Res. Atmos., 119, 9567–9577, https://doi.org/10.1002/2014JD021888., 2014.

Hennigan, C. J., Sullivan, A. P., Collett Jr, J. L., & Robinson, A. L.: Levoglucosan stability in biomass burning particles exposed to hydroxyl radicals, Geophysical Research Letters, 38(9), L09806. https://doi.org/10.1029/2011GL046686, 2011.

Heikkinen, L., Partridge, D. G., Blichner, S., Huang, W., Ranjan, R., Bowen, P., Tovazzi, E., Petäjä, T., Mohr, C., and Riipinen, I.: Cloud response to co-condensation of water and organic vapors over the boreal forest, Atmos. Chem. Phys., 24, 5117–5147, https://doi.org/10.5194/acp-24-5117-2024, 2024.

Hu, D., Topping, D., and McFiggans, G.: Measured particle water uptake enhanced by co-condensing vapours, Atmos. Chem. Physic. 18: 14925-14937, https://doi.org/10.5194/acp-18-14925-2018, 2018.

Irwin, M., Good, N., Crosier, J., Choularton, T. W., and McFiggans, G.: Reconciliation of measurements of hygroscopic growth and critical supersaturation of aerosol particles in central Germany, Atmos. Chem. Phys., 10, 11737–11752, https://doi.org/10.5194/acp-10-11737-2010, 2010.

Jaatinen, A., Romakkaniemi, S., Anttila, T., Hyvärinen, A-P., Hao, Li-Qing, Kortelainen, A., Miettinen, P., Mikkonen, S., Smith, J. N., Virtanen, A., and Laaksonen, A.: The third Pallas Cloud Experiment: Consistency between the aerosol hygroscopic growth and CCN activity, Boreal Environment Research 19 (suppl. B), 368–382, 2014.

Jimenez, J. L., Jayne, J. T., Shi, Q., Kolb, C. E., Wornosop, D. R., Yourshaw, I., Seinfeld, J. H., Flagan, R. C., Zhang, X., Smith, K. A., Morris, J. W., and Davidovits, P.: Ambient aerosol sampling using the Aerodyne aerosol spectrometer, Journal of Geophysical Research, https://doi.org/10.1029/2001JD001213, 2003.

https://doi.org/10.5194/egusphere-2026-2723
Preprint. Discussion started: 13 July 2026

Jurányi, Z., Gysel, M., Duplissy, J., Weingartner, E., Tritscher, T., Dommen, J., Henning, S., Ziese, M., Kiselev, A., Stratmann, F., George, I., and Baltensperger, U.: Influence of gas-to-particle partitioning on the hygroscopic and droplet activation behaviour of a-pinene secondary organic aerosol, Physical Chemistry Chemical Physic, 11, 8091-8097, https://doi.org/10.1039/B904162A, 2009.

Kawana, K., Nakayama, T., and Mochida, M.: Hygroscopicity and CCN activity of atmospheric aerosol particles and their relation to organics: Characteristics of urban aerosols in Nagoya, Japan, J. Geophys. Res. Atmos., 121, 4100–4121, doi:10.1002/2015JD023213, 2016.

Kim, N., Park, M., Yum, S. S., Park, J. S., Song, I. H., Shin, H. J., Ahn, J. Y., Kwak, K. H., Kim, H., Bae, G. N., Lee, G.: Hygroscopic properties of urban aerosols and their cloud condensation nuclei activities measured in Seoul during the MAPS-Seoul campaign, Atmospheric Environment, 153, 217–232, https://doi.org/10.1016/j.atmosenv.2017.01.034, 2017.

Koop, T., Bookhold, J., Shiraiwa, M., & Pöschl, U.: Glass transition and phase state of organic compounds: dependency on molecular properties and implications for secondary organic aerosols in the atmosphere, Physical Chemistry Chemical Physics, 13, 19238–19255, https://doi.org/10.1039/C1CP22617G, 2011.

Kuwata, M., Kondo, Y., and Takegawa, N.: Critical condensed mass for activation of black carbon as cloud condensation nuclei in Tokyo, Journal of Geophysical Research, 114, D20202, doi:10.1029/2009JD012086, 2009.

Laborde, M., Mertes, P., Zieger, P., Dommen, J., Baltensperger, U., and Gysel, M.: Sensitivity of the Single Particle Soot Photometer to different black carbon types, Atmospheric Measurement Techniques, 5, 1031–1043, https://doi.org/10.5194/amt-5-1031-2012, 2012.

Lambe, A. T., Onasch, T. B., Massoli, P., Croasdale, D. R., Wright, J. P., Ahern, A. T., Williams, L. R., Worsnop, D. R., Brune, W. H., and Davidovits, P.: Laboratory studies of the chemical composition and cloud condensation nuclei (CCN) activity of secondary organic aerosol (SOA) and oxidized primary organic aerosol (OPOA), Atmos. Chem. Phys., 11, 8913–8928, doi:10.5194/acp-11-8913-2011, 2011

Laskin, A., Laskin, J., & Nizkorodov, S. A.: Chemistry of atmospheric brown carbon. Chemical Reviews, 115(10), 4335–4382. https://doi.org/10.1021/cr5006167, 2015.

Levin, E. J. T., Prenni, A. J., Palm, B. B., Day, D. A., Campuzano-Jost, P., Winkler, P. M., Kreidenweis, S. M., DeMott, P. J., Jimenez, J. L., and Smith, J. N.: Size-resolved aerosol composition and its link to hygroscopicity at a forested site in Colorado, Atmos. Chem. Phys., 14, 2657-2667, https://doi.org/10.5194/acp-14-2657-2014, 2014.

Li, C., Hu, Y., Chen, J., Ma, Z., Ye, X., Yang, X., Wang, L., Wang, X., Mellouki, A.: Physiochemical properties of carbonaceous aerosol from agricultural residue burning: Density, volatility, and hygroscopicity, Atmospheric Environment, 140, 94-105, https://doi.org/10.1016/j.atmosenv.2016.05.052, 2016.

https://doi.org/10.5194/egusphere-2026-2723
Preprint. Discussion started: 13 July 2026

Li, C., He, Q., Schade, J., Passig, J., Zimmermann, R., Meidan, D., Laskin, A., Rudich, Y., & Pöschl, U.: Dynamic changes in optical properties and chemical composition of biomass burning organic aerosol due to photochemical aging. Atmospheric Chemistry and Physics. 19(11): 7319–7342. https://doi.org/10.5194/acp-19-7319, 2019.

Liu, D., Whitehead, J., Alfarra, M. R., Reyes-Villegas, E., Spracklen, D. V., Reddington, C. L., Kong, S., Williams, P. I., Ting, Y. C., Haslett, S., Taylor, J. W., Allan, J. D., Coe, H., & McFiggans, G.: Black-carbon absorption enhancement in the atmosphere determined by particle mixing state, Nature Geoscience, 10(3), 184–188. https://doi.org/10.1038/ngeo2901, 2013.

Liu, D., Whitehead, J., Alfarra, M., Reyes-Villegas, E., Sparcklen, D. V., Reddington, C. L., Kong, S., Williams, P. I., Ting, Yu-Chieh, Hasslet, S., Taylor, J. W., Flynn, M. J., Morgan, W. T., McFiggans, G., Coe, H., Allan, J. D.: Black-carbon absorption enhancement in the atmosphere determined by particle mixing state, Nature Geoscience, 10, 184-188, https://doi.org/10.1038/ngeo2901, 2017.

Li, R., Li, S., Jiang, X., Wu, Y., Hu, K.: Organic Vapors from Residential Biomass Combustion: Emission Characteristics and Conversion to Secondary Organic Aerosols, Atmosphere, 15, 692, https://doi.org/10.3390/atmos15060692, 2024.

Markelj, J., Madronich, S., & Pompe, M.: Modeling of hygroscopicity parameter κ of organic aerosols using quantitative structure-property relationships, J Atmos Chem, 74, 357–376, https://doi.org/10.1007/s10874-016-9347-3, 2017.

Mei, F., Zhang, Q., Setyan, A., Xu, L., Lin, Y., Wang, J., and Zhang, R. J.: CCN activity and mixing state of urban and biomass burning aerosols in the southeastern US. Atmospheric Chemistry and Physics. 13(23): 12155–12174. https://doi.org/10.5194/acp-13-12155-2013, 2013.

Mikhailov E, Vlasenko S, Martin ST, Koop T, Pöschl U.: Amorphous and crystalline aerosol particles interacting with water vapor: conceptual framework and experimental evidence for restructuring, phase transitions and kinetic limitations, Atmospheric Chemistry and Physics, 9, 9491–9522. https://doi.org/10.5194/acp-9-9491-2009, 2009.

Mikhailov, E. F., Mironov, G. N., Pöhlker, C., Chi, X., Krüger, M. L., Shiraiwa, M., Förster, J. D., Pöschl, U., Vlasenko, S. S., Ryshkevich, T. I., Weigand, M., Kilcoyne, A. L. D., and Andreae, M. O.: Chemical composition, microstructure, and hygroscopic properties of aerosol particles at the Zotino Tall Tower Observatory (ZOTTO), Siberia, during a summer campaign, Atmos. Chem. Phys., 15, 8847–8869, doi:10.5194/acp-15-8847-2015, 2015.

Mori, T., Kondo, Y., Ohata, S., Moteki, N., Matsui, H., Oshima, N., Iwasaki, A.: Wet deposition of black carbon at a remote site in the East China Sea, J. Geophys. Res. Atmos., 119, 10485–10498, doi:10.1002/ 2014JD022103, 2014.

Müller, A., Y. Miyazaki, S. G. Aggarwal, Y. Kitamori, S. K. R. Boreddy, and K. Kawamura: Effects of chemical composition and mixing state on size-resolved hygroscopicity and cloud condensation nuclei activity of submicron aerosols at a suburban site in northern Japan in summer, J. Geophys. Res. Atmos., 122, 9301–9318, doi:10.1002/2017JD027286, 2017.

Noyes, K. T. J., Kahn, R. A., Limbacher, J. A., and Li, Z.: Canadian and Alaskan wildfire smoke particle properties, their evolution, and controlling factors, from satellite observations, Atmos. Chem. Phys., 22, 10267–10290, https://doi.org/10.5194/acp-22-10267-2022, 2022.

https://doi.org/10.5194/egusphere-2026-2723
Preprint. Discussion started: 13 July 2026

Oghama, O. E., Voliotis, A., Bannan, T. J., Syafira, S. A., Hu, D., Wu, H., Gallimore, P., McFiggans, G., Coe, H., and Allan, J. D.: Variations in oxygenated and nitrogen-containing primary organic compounds based on the fuel type and burning condition in stove emissions, Environmental Science: Atmosphere, 5, 1297-1311, DOI: 10.1039/d5ea00080g, 2025.

Oghama, O. E., Voliotis, A., Bannan, T. J., Syafira, S. A., Hu, D., Wu, H., Gallimore, P., Matthews, E., McFiggans, G., Coe, H., and Allan, J. D.: Effect of photochemical aging on biomass burning emissions: contributions of oxidized organic nitrogen from a variety of biomass types, *ACS Earth Space Chem.*, https://doi.org/10.1021/acsearthspacechem.6c00093, 2026

Petters, M. D., & Kreidenweis, S. M.: A single parameter representation of hygroscopic growth and cloud condensation nucleus activity, Atmospheric Chemistry and Physics., 7(8), 1961-1971, https://doi.org/10.5194/acp-7-1961-2007, 2007.

Petters, M. D., Carrico, C. M., Kreidenweis, S. M., Prenni, A. J., DeMott, P. J., Collett, J. L., & Moosmüller, H.: Cloud condensation nucleation activity of biomass burning aerosol. Journal of Geophysical Research: Atmospheres, 114, D22205. https://doi.org/10.1029/2009JD012353, 2009.

Pajunoja, A., Lambe, A., Hakala, J., Rastak, N., Cummings, M., Brogan, J., Hao, L., Paramonov, M., Hong, J., Prisle, N., Malila, J., Romakkaniemi, S., Lehtinen, K., Laaksonen, A., Kulmala, M., Massoli, P., Onasch, T., Donahue, N., Riipinen, I., Davidovits, P., Worsnop, D., Petäjä, T., & Virtanen, A.: Adsorptive uptake of water by semisolid secondary organic aerosols, Geophysical Research Letters, 42, 3063 - 3068. https://doi.org/10.1002/2015gl063142, 2015.

Pöhlker M. L., Pöhlker, C., Quaas, J., Mülmenstädt, J., Pozzer, A., Andreae, M. O., Artaxo, P., Block, K., Coe, H., Ervens, B., Gallimore, P., Gaston, C. J., Gunthe, S. S., Henning, S., Herrmann, H., Krüger, O., McFiggans, G., Poulain, L., Raj, S. S., Reyes-Villegas, E., Royer, H. M., Walter, D., Wang, Y., Pöschl, U.: Global organic and inorganic aerosol hygroscopicity and its effect on radiative forcing, Nat Commun, 14, 6139, 2023.

Ravichandran, E., Han, S., Williams, A. S., Berta, V., Dedrick, J. L., Pelayo, C., Maneenoi, N., Russel, L. M., Wheeler, M., Wentzell, J., Liggio, J., and Petters, M.: Removal of trace gases can both increase and decrease cloud droplet formation, Science Advances, 12(3), DOI: 10.1126/sciadv.adx0960, 2026.

Reid, J. S., Koppmann, R., Eck, T. F., and Eleuterio, D. P.: A review of biomass burning emissions part II: intensive physical properties of biomass burning particles, J. Geophys. Res., 110, D18206. https://doi.org/10.1029/2005JD005783, 2025.

Reilly, P. J. and Wood, R. H.: Prediction of properties of mixed electrolytes from measurements on common ion mixtures, J. Phys. Chem., 73, 4292–4297, 1969

Roberts, G. C., & Nenes, A.: A Continuous-Flow Streamwise Thermal-Gradient CCN Chamber for Atmospheric Measurements, Aerosol Science and Technology, 39(3), 206–221. https://doi.org/10.1080/027868290913988, 2005.

Rose, D., Gunthe, S., Mikhailov, E., Frank, G., Dusek, U., Andreae, M., Pöschl, U.: Calibration and measurement uncertainties of a continuous-flow cloud condensation nuclei counter (DMT-CCNC): CCN activation of ammonium sulfate and sodium chloride aerosol particles in theory and experiment, Atmos. Chem. Phys., 8, 1153-1179. https://doi.org/10.5194/acp-8-1153-2008, 2008.

Rose, D., Gunthe, S. S., Su, H., Garland, R. M., Nowak, A., Achtert, P., Wiedensohler, A., Andreae, M. O., & Pöschl, U. (2010). Cloud condensation nuclei in polluted air and biomass burning smoke near the mega-city Guangzhou, China – Part 1: Size-resolved measurements and implications for the modeling of aerosol particle hygroscopicity and CCN activity. Atmospheric Chemistry and Physics. 10(7): 3365-3383. https://doi.org/10.5194/acp-10-3365-2010.

Rose, D., Gunthe, S. S., Mikhailov, E., Frank, G. P., Dusek, U., Andreae, M. O., & Pöschl, U. (2010). Cloud condensation nuclei activity of soot particles, Atmospheric Chemistry and Physics, 10, 3365–3377. https://doi.org/10.5194/acp-10-3365-2010

Saleh, R., Hennigan, C. J., McMeeking, G. R., Chuang, W. K., Robinson, E. S., Coe, H., Donahue, N. M., and Robinson, A. L.: Absorptivity of brown carbon in fresh and photo-chemically aged biomass-burning emissions, Atmospheric chemistry and physics, 13, 7683–7693, https://doi.org/10.5194/acp-13-7683-2013, 2013.

Sapkal, M. G., Rosch, M., and Kanji, Z. A.: Development of the horizontal cloud condensation nuclei counter (HCCNC) to detect particle activation down to 4 C temperature and 0.05% supersaturation, Atmospheric Measurement Techniques, 18, 5649-5667, https://doi.org/10.5194/amt-18-5649-2025, 2025.

Shao, Y., Wang, Y., Du, M., Voliotis, A., Alfarra, M. R., O'Meara, S. P., Turner, S. F., and McFiggans, G.: Characterization of the Manchester Aerosol Chamber facility, Atmos. Meas. Tech., 15, 539–559, https://doi.org/10.5194/amt-15-539-2022, 2022.

Stefenelli, G., Jiang, J., Bertrand, A., Bruns, E. A., Pieber, S. M., Baltensperger, U., Marchand, N., Aksoyoglu, S., Prévôt, A. S. H., Slowik, J. G., and El Haddad, I.: Secondary organic aerosol formation from smouldering and flaming combustion of biomass: a box model parametrization based on volatility basis set, Atmos. Chem. Phys., 19, 11461–11484, https://doi.org/10.5194/acp-19-11461-2019, 2019.

Syafira, S. A., Effendi, M. D., Romadhon, M. S.: Comparative review of laboratory approaches for simulating and characterizing aerosol emissions from open biomass burning, Environmental Science: Atmosphere, Advance Article, DOI: https://doi.org/10.1039/D5EA00146C, 2026.

Swietlicki, E., H.-C. Hansson, K. Hämeri, B. Svenningsson, A. Massling, G. McFiggans, P. H. McMurry, T. Petäjä, P. Tunved, M. Gysel, D. Topping, E. Weingartner, U. Baltensperger, J. Rissler, A. Wiedensohler & M. Kulmala: Hygroscopic Properties of Sub-Micrometer Atmospheric Aerosol Particles Measured with H-TDMA Instruments in Various Environments – A Review, Tellus-B (Chemical & Physical Meteorology), **60**, 3, 432-469, doi:10.1111/j.1600-0889.2008.00350.x, 2008

Tang, M., Chan, C. K., Li, Y. J., Su, H., Ma, Q., Wu, Z., Zhang, G., Wang, Z., Ge, M., Hu, M., He, H., and Wang, X.: A review of experimental techniques for aerosol hygroscopicity studies, Atmospheric Chemistry and Physics, 19, 12631–12686, https://doi.org/10.5194/acp-19-12631-2019, 2019.

Tao, J., Kuang, Y., Ma, N., Zheng, Y., Wiedensohler, A., and Zhao, C.: An improved parameterization scheme for size-resolved particle activation ratio and its application on comparison study of particle hygroscopicity measurements

https://doi.org/10.5194/egusphere-2026-2723
Preprint. Discussion started: 13 July 2026

between HTDMA and DMA-CCNC, Atmospheric Environment, 226: 117403. https://doi.org/10.1016/j.atmosenv.2020.117403, 2020.

Tao, J., Luo, B., Xu, W., Zhao, G., Xu, H., Xue, B., Zhai, M., Xu, W., Zhao, H., Ren, S., Zhou, G., Liu, L., Kuang, Y., and Sum, Y.: Markedly different impacts of primary emissions and secondary aerosol formation on aerosol mixing states revealed by simultaneous measurements of CCNC, H(/V)TDMA, and SP2, Atmos. Chem. Phys., 24, 9131–9154, https://doi.org/10.5194/acp-24-9131-2024, 2024.

Taylor, J. W., Allan, J. D., Liu, D., Flynn, M., Weber, R., Zhang, X., Lefer, B. L., Grossberg, N., Flynn, J., and Coe, H.: Assessment of the sensitivity of core/shell parameters derived using the single-particle soot photometer to density and refractive index, Atmospheric Measurement Techniques, 8, 1701–1718, https://doi.org/10.5194/amt-8-1701-2015, 2015.

Thalman, R., de Sá, S. S., Palm, B. B., Barbosa, H. M. J., Pöhlker, M. L., Alexander, M. L., Brito, J., Carbone, S., Castillo, P., Day, D. A., Kuang, C., Manzi, A., Ng, N. L., Sedlacek III, A. J., Souza, R., Springston, S., Watson, T., Pöhlker, C., Pöschl, U., Andrea, M. O., Artaxo, P., Jimenez, J. L., Martin, S. T., and Wang, J.: CCN activity and organic hygroscopicity of aerosols downwind of an urban region in central Amazonia: seasonal and diel variations and impact of anthropogenic emissions, Atmos. Chem. Phys., 17, 11779–11801, https://doi.org/10.5194/acp-17-11779-2017, 2017.

Topping, D. O., McFiggans, G. B., and Coe, H.: A curved multi-component aerosol hygroscopicity model framework: Part 2 – Including organic compounds, Atmos. Chem. Phys., 5, 1223–1242, https://doi.org/10.5194/acp-5-1205-2005, 2005.

Topping, D., Connoly, P., and McFiggans, G.: Cloud droplet number enhanced by co-condensation of organic vapours, Nature Geoscience, 6, 443-446, https://doi.org/10.1038/ngeo1809, 2013.

Vokes, E. T., Lewis, E. R., Johnson, A. L., and Cotterell, M. I.: Densities of internally mixed organic-inorganic particles from mobility diameter measurements of aerodynamically classified aerosols, Aerosol Science and Technology, 56, 688–710, https://doi.org/10.1080/02786826.2022.2062293, 2022.

Vu, D., Gao, S., Berte, T., Kacarab, M., Yao, Q., Vafai, K., and Asa-Awuku, A.: External and internal cloud condensation nuclei (CCN) mixtures: controlled laboratory studies of varying mixing states, Atmos. Meas. Tech., 12, 4277–4289, https://doi.org/10.5194/amt-12-4277-2019, 2019.

Wang, W., Lei, T., Zuend, A., Su, H., Cheng, Y., Shi, Y., Ge, M., and Liu, M.: Effect of mixing structure on the water uptake of mixtures of ammonium sulfate and phthalic acid particles, Atmospheric chemistry and physics, 21, 2179–2190, https://doi.org/10.5194/acp-21-2179-2021, 2021.

Wang, X., Ye, X., Chen, J., Wang, X., Yang, X., Fu, T.-M., Zhu, L., and Liu, C.: Direct links between hygroscopicity and mixing state of ambient aerosols: estimating particle hygroscopicity from their single-particle mass spectra, Atmos. Chem. Phys., 20: 6273–6290, https://doi.org/10.5194/acp-20-6273-2020, 2020.

Wang, Y., Luo, B., Kleinheins, J., Chen, G. I., Heikkinen, L., and Marcolli, C.: Cloud droplet number enhancement from co-condensing NH3, HNO3, and organic vapours: boreal case study, Atmos. Chem. Phys, 26, 1735-1749, https://doi.org/10.5194/acp-26-1735-2026, 2025.

https://doi.org/10.5194/egusphere-2026-2723
Preprint. Discussion started: 13 July 2026

Wang, Y., Wang, Y., Song, X., Shang, Y., Zhou, Y., Huang, X., and Li, Z.: The impact of particulate pollution control on aerosol hygroscopicity and CCN activity in North China, Environmental Research Letters, 18, 074028, **DOI** 10.1088/1748-9326/acde91, 2023.

Wang, Y., Voliotis, A., Hu, D., Shao, Y., Du, M., Chen, Y., Kleinheins, J., Marcolli, C., Alfarra, M. R., and McFiggans, G.: On the evolution of sub- and super-saturated water uptake of secondary organic aerosol in chamber experiments from mixed precursors, Atmos. Chem. Phys., 22, 4149–4166, https://doi.org/10.5194/acp-22-4149-2022, 2022.

Ward-Baranyay, M., Lee, C., Pascolini-Campbell, M., Sousa, D., & Kinoshita, A. M. (2026). Pre-fire fuel conditions are dominant drivers of burn severity in the 2025 Los Angeles County fires. AGU Advances, 7, e2025AV002179. https://doi.org/10.1029/2025AV002179

Wex, H., Petters, M. D., Carrico, C. M., Hallbauer, E., Massling, A., McMeeking, G. R., Poulain, L., Wu, Z., Kreidenweis, S. M., and Stratmann, F.: Towards closing the gap between hygroscopic growth and activation for secondary organic aerosol: Part 1- Evidence from measurements, Atmospheric Chemistry Physic, 9, 3987-3997, https://doi.org/10.5194/acp-9-3987-2009, 2009.

Wokosin, K. A., Schell, E. L., and Faust, J. A.: Emerging investigator series: surfactants, films, and coatings on atmospheric aerosol particles: a review, Environmental Science: Atmospheres, 2, 775, https://doi.org/10.1039/D2EA00003B, 2022.

Wu, L., Ro, CU.: Aerosol Hygroscopicity on A Single Particle Level Using Microscopic and Spectroscopic Techniques: A Review. Asian J. Atmos. Environ., 14, 177–209, https://doi.org/10.5572/ajae.2020.14.3.177, 2020.

Wu, Z. J., Poulain, L., Henning, S., Dieckmann, K., Birmili, W., Merkel, M., Pinxteren, D., Spindler, G., Müller, K., Stratmann, F., Herrmann, H., & Wiedensohler, A.: Relating particle hygroscopicity and CCN activity to chemical composition during the HCCT-2010 field campaign, Atmospheric Chemistry and Physics, 13, 7983-7996, https://doi.org/10.5194/acp-13-7983-2013, 2013.

Wu, Z. J., Zheng, J., Shang, D. J., Du, Z. F., Wu, Y. S., Zeng, L. M., Wiedensohler, A., and Hu, M.: Particle hygroscopicity and its link to chemical composition in the urban atmosphere of Beijing, China, during summertime, Atmos. Chem. Phys., 16, 1123-1138, https://doi.org/10.5194/acp-16-1123-2016, 2016.

Xiong, C., Chen, X., Ding, X., Kuang, B., Pei, X., Xu, Z., Yang, S., Hu, H., and Wang, Z.: Reconsideration of surface tension and phase state effects on cloud condensation nuclei activity based on the atomic force microscopy measurement, Atmospheric chemistry and physics, 22, 16123–16135, https://doi.org/10.5194/acp-22-16123-2022, 2022.

Xu, W., Fossum, K. N., Ovadnevaite, J., Lin, C., Huang, R.-J., O'Dowd, C., and Ceburnis, D.: The impact of aerosol size-dependent hygroscopicity and mixing state on the cloud condensation nuclei potential over the north-east Atlantic, Atmos. Chem. Phys., 21, 8655–8675, https://doi.org/10.5194/acp-21-8655-2021, 2021.

Zardini, A. A., Sjogren, S., Marcolli, C., Krieger, U. K., Gysel, M., Weingartner, E., Baltensperger, U., & Peter, T.: A combined particle trap/HTDMA hygroscopicity study of mixed inorganic/organic aerosol particles, Atmospheric Chemistry and Physics, 8(18), 5589-5601, https://doi.org/10.5194/acp-8-5589-2008, 2008.

https://doi.org/10.5194/egusphere-2026-2723
Preprint. Discussion started: 13 July 2026

Zhang, C., Lu, M., Ma, N., Yang, Y., Wang, Y., Größ, J., Fan, Z., Wang, M., & Wiedensohler, A.: Hygroscopicity of aerosol particles composed of surfactant SDS and its internal mixture with ammonium sulfate at relative humidities up to 99.9%, Atmospheric Environment, 298, 119625-119635, https://doi.org/https://doi.org/10.1016/j.atmosenv.2023.119625, 2023.

Zhang, X., and Mao, M.: Radiative properties of coated black carbon aerosols impacted by their mycrophysics, Journal of Quantitative Spectroscopy & Radiative Transfer, 241, 106718-106728, https://doi.org/10.1016/j.jqsrt.2019.106718, 2020.

Zhang, Y., Chen, Y., Lambe, A. T., Davidovits, P., Onasch, T. B., Worsnop, D. R., & Zhang, Q.: Effect of black carbon mixing state on the hygroscopicity and optical properties of submicron aerosols, Environmental Science & Technology, 54(15), 9490–9501, https://doi.org/10.1021/acs.est.0c01801, 2020.